Miner Deposita (2007) 42:175–204
DOI 10.1007/s00126-006-0106-2

ARTICLE

Lode–gold mineralization in the Tanami region, northern Australia

David L. Huston · Leon Vandenberg · Andrew S. Wygralak · Terrence P. Mernagh · Leon Bagas · Andrew Crispe · Alexis Lambeck · Andrew Cross · Geoff Fraser · Nick Williams · Kurt Worden · Tony Meixner · Bruce Goleby · Leonie Jones · Pat Lyons · David Maidment

Received: 1 January 2006 / Accepted: 11 October 2006 / Published online: 15 November 2006

Abstract The Tanami region of northern Australia has emerged over the last two decades as the largest gold-producing region in the Northern Territory. Gold is hosted by epigenetic quartz veins in sedimentary and mafic rocks, and by sulfide-rich replacement zones within iron formation. Although limited, geochronological data suggest that most mineralization occurred at about 1,805–1,790 Ma, during a period of extensive granite intrusion, although structural relationships suggest that some deposits predate this period. There are three main goldfields in the Tanami region: the Dead Bullock Soak goldfield, which hosts the world-class Callie deposit; The Granites goldfield; and the Tanami goldfield. In the Dead Bullock Soak goldfield, deposits are hosted by carbonaceous siltstone and iron formation where a late (D_5) structural corridor intersects an early F_1 anticlinorium. In The Granites goldfield, deposits are hosted by highly sheared iron formation and are interpreted to predate D_5. The Tanami goldfield consists of a large number of small, mostly basalt-hosted deposits that probably formed at a high structural level during D_5. The D_5 structures that host most deposits formed in a convergent structural regime with σ_1 oriented between E–W and ENE–WSW. Structures active during D_5 include NE-trending oblique thrust (dextral) faults and ESE-trending (sinistral) faults that curve into N- to NNW-trending reverse faults localized in supracrustal belts between and around granite complexes. Granite intrusions also locally perturbed the stress field, possibly localizing structures and deposits. Forward modeling and preliminary interpretations of reflection seismic data indicate that all faults extend into the mid-crust. In areas characterized by the N- to NW-trending faults, orebodies also tend to be N- to NW-trending, localized in dilational jogs or in fractured, competent rock units. In areas characterized by ESE-trending faults, the orebodies and veins tend to strike broadly east at an angle consistent with tensional fractures opened during E–W- to ENE–WSW-directed transpression. Many of these deposits are hosted by reactive rock units such as carbonaceous siltstone and iron formation. Ore deposition occurred at depths ranging from 1.5 to 11 km from generally low to moderate salinity carbonic fluids with temperatures from 200 to 430°C, similar to lode–gold fluids elsewhere in the world. These fluids are interpreted as the product of metamorphic dewatering caused by enhanced

Editorial handling: L. Meinert

D. L. Huston (✉) · T. P. Mernagh · A. Lambeck · A. Cross · G. Fraser · N. Williams · K. Worden · T. Meixner · B. Goleby · L. Jones · P. Lyons · D. Maidment
Geoscience Australia,
GPO Box 378, Canberra, ACT 2601, Australia
e-mail: David.Huston@ga.gov.au

L. Vandenberg · A. Crispe
Northern Territory Geological Survey,
P.O. Box 8760, Alice Springs, NT 0871, Australia

A. S. Wygralak
Northern Territory Geological Survey,
GPO Box 3000, Darwin, NT 0801, Australia

L. Bagas
Geological Survey of Western Australia,
100 Plain St,
East Perth, WA 6009, Australia

L. Bagas
Centre for Exploration Targeting,
University of Western Australia,
Crawley, WA 6004, Australia

heat flow, although it is also possible that the fluids were derived from coeval granites. Lead isotope data suggest that lead in the ore fluids had multiple sources. Hydrogen and oxygen isotope data are consistent with both metamorphic and magmatic origins for ore fluids. Gold deposition is interpreted to be caused by fluid unmixing and sulfidation of host rocks. Fluid unmixing is caused by three different processes: (1) CO_2 unmixing caused by interaction of ore fluids with carbonaceous siltstone; (2) depressurization caused by pressure cycling in shear zones; and (3) boiling as ore fluids move to shallow levels. Deposits in the Tanami region may illustrate the continuum model of lode–gold deposition suggested by Groves (Mineralium Deposita 28:366–374, 1993) for Archean districts.

Keywords Lode–gold · Tanami · Paleoproterozoic · Mineral system

The Tanami region: a history of discovery, mining, and the evolution of genetic models

The Tanami region (Figs. 1 and 2) has emerged as an important Paleoproterozoic gold provinces over the last two decades. Although gold prospects were identified as early as 1900 (Davidson 1905), production was sporadic until the mid- to late 1980s with total production of about 540 kg (Plumb 1990). Since the mid-1980s, mines were developed in The Granites (1986, Mayer 1990), Tanami (1987, Nicholson 1990), Dead Bullock Soak goldfields (1990, Smith et al. 1998), and at the Groundrush (2001), Minotaur (2003) and Coyote (2006) deposits. In addition, significant resources have been identified at the Oberon, Crusade, Sandpiper and Kookaburra prospects (Fig. 2).

Before the late 1930s, exploration in the Tanami region was limited to prospecting, with a minor gold rush in the Tanami district from 1908 to 1913 (Nicholson 1990; Mayer 1990). Between the late 1930s and early 1980s, activity was limited to geophysical surveys in The Granites and Tanami goldfields (Hossfeld 1940a,b; Daly 1962), with sporadic exploration and very limited gold production. Modern exploration commenced in the early to mid-1980s around known prospects in The Granites and Tanami goldfields. This exploration yielded rapid results, with development of mines less than 5 years after exploration commenced. In 1988, initial exploration in the Dead Bullock Soak goldfield returned near-surface grades up to 10 g/t. By June 1989, a resource of 0.6 Mt grading 3.3 g/t Au was defined at the Triumph Hill and Dead Bullock Ridge deposits, with mine development commencing in 1990 (Smith et al. 1998).

The most significant discovery in the Tanami region was the Callie deposit. This deposit was discovered in 1991 under shallow (7 m) cover, approximately 2 km to the west of the Triumph Hill and Dead Bullock Ridge deposits. Based on the recognition that deposits in the Dead Bullock Soak goldfield were located within the axial corridor of a major anticlinorium, vacuum drilling to bedrock yielded a sinuous bedrock gold anomaly (>50 ppb) with a peak of 7 ppm (Smith et al. 1998).

Two of the most recent discoveries in the Tanami region highlight two factors that have hindered exploration: land access and regolith cover. The outcropping Groundrush deposit was discovered only 7 weeks after initial sampling after the miners were granted land access, and the Coyote deposit was discovered under 10–40 m of transported overburden.

The models for the genesis of gold deposits in the Tanami region have evolved over the two decades of modern exploration. Initial models for the genesis of deposits in The Granites goldfield invoked syngenetic gold deposition associated with submarine hot springs (Ireland and Mayer 1984), in line with genetic concepts prevalent at the time (e.g., Hodgson and MacGeehan 1982). Although an epigenetic origin for deposits in the Tanami region is now generally accepted, debate about the role of magmas in ore genesis still exists. Some recent authors have inferred that the ore-forming fluids were metamorphic in origin (Mayer 1990; Nicholson 1990; Smith et al. 1998), although perhaps driven by a granitic intrusion. Alternatively, Wall and Taylor (1990), Tunks and Marsh (1998), and Wall (2005) invoked a mixed magmatic–metamorphic origin for the gold, with the fluids derived from the thermal aureole of nearby granites.

The tectonic setting and timing of gold mineralization in northern Australia

Gold deposits in northern Australia along with gold deposits in the Trans-Hudson Orogen of North America are the main contributors to a major Paleoproterozic concentration of gold deposits. Collectively, these deposits, which produced in excess of 2,100 tonnes (70 MOz) of gold (Goldfarb et al. 2001: reserves and production), have been constrained to between ~1,820 and ~1,730 Ma (Goldfarb et al. 2001; as updated using geochronological data from Şener et al. 2005; Cross et al. 2005; Morelli et al. 2005; Rasmussen et al. 2006; Bagas et al. 2006). Based on xenotime sensitive high resolution ion microprobe (SHRIMP) U–Pb data and $^{40}Ar/^{39}Ar$ data of Fraser (2002), Şener et al. (2005) proposed a single gold event in northern Australia at 1,750–1,730 Ma, extending from the Ashburton basin in the West Australian Craton to the Tanami and Pine Creek regions in the North Australian Craton. More recent data (Cross et al. 2005; Rasmussen et al. 2006; Bagas et al. 2006; see discussion below) suggest that this is not a single event, with most gold mineralization in the Tanami and Pine Creek regions occurring synchro-

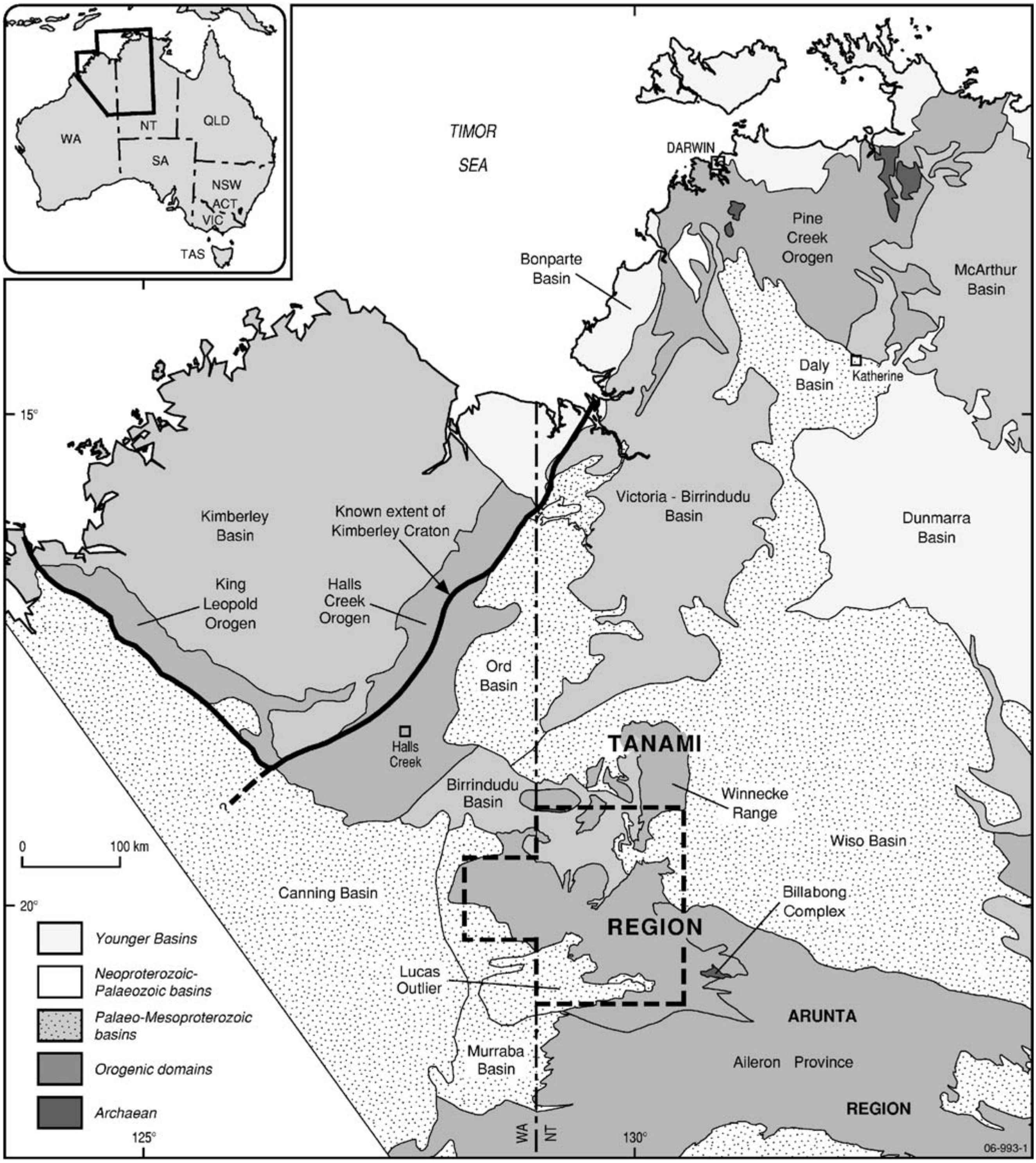

Fig. 1 Map showing major crustal elements of the northwestern North Australian Craton. The *boxed area* shows the location of Figs. 2 and 3

nously (within error) between ~1,805 and ~1,780 Ma, possibly related to the same tectonic event.

The first thermotectonic event shared by the Tanami, Halls Creek, and Pine Creek regions is bracketed between ~1,835 and ~1,825 Ma. In the Halls Creek and Pine Creek regions, this event is known as the Halls Creek Orogeny (Blake et al. 2000) and Maud Creek event, respectively (Stuart-Smith et al. 1993; new age constraints from Jagodzinki 1998), and produced north to north–east trending folds and fabrics. These structural orientations are consistent with the interpretation of Sheppard et al. (1999, 2001) that this event marks the docking of the Kimberley

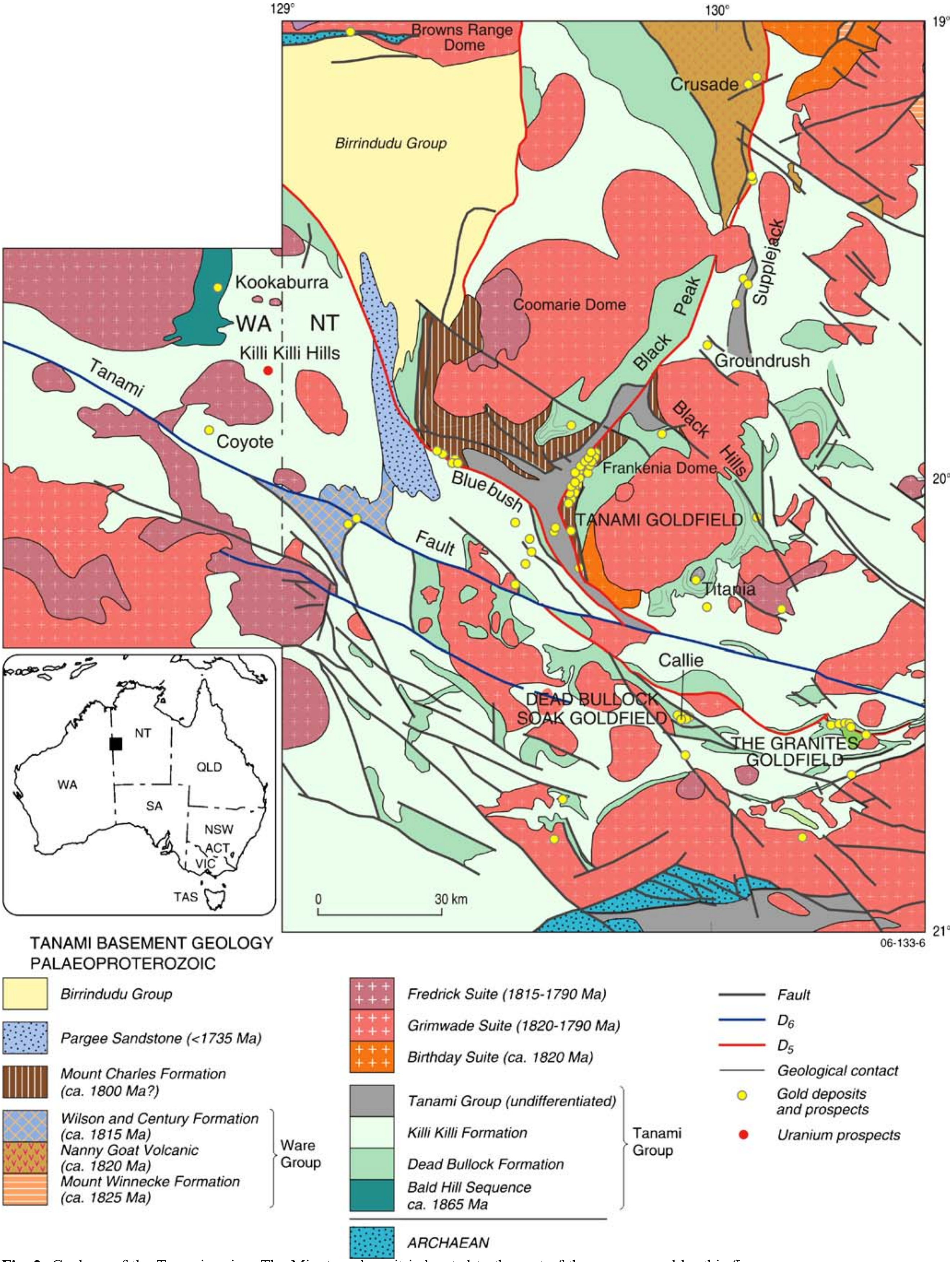

Fig. 2 Geology of the Tanami region. The Minotaur deposit is located to the east of the area covered by this figure

Craton onto the North Australia Craton (Fig. 1); deformation in the Tanami and Pine Creek regions may reflect migration of stresses caused by collision. In the Tanami region, the Tanami Event is characterized by southeast to east trending folds (Crispe et al. 2006; see below), orientations different to those of similar age structures in the Halls Creek and Pine Creek regions. This difference is likely the result of later folding and perturbations in the stress field caused by the location of the Tanami region south of the main collision zone (Fig. 1).

Between ~1,835 and ~1,795 Ma, all three regions are characterized by extensive magmatism (Stuart-Smith et al. 1993; Blake et al. 2000; see below), with magmatism in the Halls Creek and Pine Creek regions beginning earlier than that in the Tanami region. Folding accompanied granite intrusion in the Halls Creek, Pine Creek, and Tanami regions (Blake et al. 2000; Stuart-Smith et al. 1993; Crispe et al. 2006). Locally voluminous mafic magma was emplaced in extensional basins towards the end of this period in the Tanami and Halls Creek regions and in the Kimberley Basin (Crispe et al. 2006; Blake et al. 2000). This magmatism may be associated with post-collisional extension after docking of the Kimberley region.

Available data suggest that gold mineralization took place near the end (Tanami region) or after (Pine Creek region) this period of magmatism and post-collisional extension. Although not well-constrained (see below), structural data from the Tanami region are consistent with gold forming in an ENE–WSW-directed convergent tectonic setting, possibly involving a component of oblique transcurrent movement. The implied change in tectonic stresses may have been caused by changes in far field stress to the south. Many of the deposits in the Pine Creek region are associated with northwest-trending strike–slip faults (e.g., Pine Creek Shear Zone) that were active during the Shoobridge Event, which, with an age of ~1,780 Ma (Stuart-Smith et al. 1993), coincides with the age of mineralization. These faults could also have formed in an oblique transcurrent tectonic regime. If this is the case, a change in tectonic environment to a transpressive environment along the suture between the Kimberley region and the North Australian Craton may have triggered gold mineralization.

Geology of the Tanami region

As Crispe et al. (2006) and Cross and Crispe (2006) describe the characteristics, relationships, and ages of supracrustal rock units and granites in the Tanami region, only a summary based on the above references is provided herein. Figure 2 shows the distribution of geologic units and regional faults, and Table 1 summarizes the characteristics of the rock units and structural elements in the context of the geologic evolution of the Tanami region.

The oldest rocks in the Tanami region are high-grade metasedimentary[1] rocks and leucogranites of Neoarchean age (~2,514±3 Ma) that occur within the Billabong Complex (located to the east of Fig. 2) and, possibly, the Browns Range Dome. Archean rocks have a very limited extent in the Tanami, although Nd isotope data suggest a more extensive distribution at depth (Page et al. 1995).

The oldest known Paleoproterozoic rocks are the Bald Hill sequence in Western Australia. This unit, which contains basalt and turbiditic rocks, was intruded by dolerite, which may have fed basalt flows, and minor, high level rhyodacite, which has been dated at 1,864±3 Ma (D. Maidment, unpublished data).

The most extensive unit is the 1,838±6-Ma (Cross et al. 2005) Tanami Group, which is subdivided into the basal Dead Bullock and overlying Killi Killi Formations. Graphitic units and banded iron formation of the Callie Member of the Dead Bullock Formation host most lode–gold deposits in the Tanami region. The Killi Killi Formation, which consists of turbiditic siliciclastic rocks, also hosts gold but is less extensively mineralized. Dolerite sills, some of which have peperitic contacts with the enclosing sedimentary rocks, intrude the Tanami Group.

Although the poor exposure precludes definitive statements, the Dead Bullock Formation seems to be restricted to the eastern and central part of the Tanami region, barely extending over the border into Western Australia (Fig. 2). This suggests that the Tanami basin was deepest in the east-central part of the basin, a hypothesis supported by provenance data from the coarser-grained Killi Killi Formation, indicating that it was sourced from the Kimberley region to the west (Cross and Crispe 2006). Crispe and Vandenberg (2004) suggest that the Supplejack Fault Zone, which is located in the eastern part of the Tanami basin, may have been active during development of the basin. As the Dead Bullock Formation is not known east of this fault, it may have formed the eastern margin of the deepwater depocenter into which the Dead Bullock Formation was deposited.

The close association of many deposits and prospects with carbonaceous and Fe-rich units in the Tanami Group suggests that the original architecture of the Tanami basin influenced the later lode–gold mineral system. Either the unusual composition of these fine-grained rocks localized gold deposition or structures developed during basin formation were reactivated during later lode–gold events.

Rocks of the Tanami Group have been affected by the ~1,830-Ma Tanami Event (D_1–M_1), which involved dis-

[1] Only rocks of amphibolite grade or higher are referred to using the prefix "meta-."

Table 1 Sedimentation, magmatic and deformation/metamorphic events in the Tanami region (data from Crispe and Vandenberg 2006; Green 2006; Crispe et al. 2006; Cross and Crispe 2006)

Period (Ma)	Sedimentation events	Magmatic events	Deformational/metamorphic events
1,735–1,640	Birrindudu Group *Coomarie Sandstone* Sublithic sandstone and quartz arenite *Talbot Wells Formation* Silicified carbonate with minor sandstone, siltstone and shale *Gardiner Sandstone* Sublithic to lithic sandstone and quartz arenite, with lesser shale and siltstone and basal conglomerate; maximum depositional age ~1,815 Ma	*Mafic sill?* Magnetic data indicate presence of 200-m thick sill in Coomarie Sandstone; age is unknown	D_{6+} Late thrust, oblique-slip and normal faults that cut earlier structures; ages poorly constrained, but likely <1,700 Ma, possibly as young as the Alice Springs Orogeny (450–300 Ma)
1,810–1,730	*Pargee Sandstone* Interbedded conglomerate, quartz arenite and minor siltstone; maximum depositional age ~1,735 Ma	*Fiddlers Lake Granite* S-type granite and migmatites in Arunta region just to SE of Tanami region; ~1,730 Ma	
1,820–1,790	*Mount Charles Formation* Fine-grained turbiditic sedimentary rocks with basal quartzose sandstone and interbedded with basalt; ?1,800–?1,790 Ma	*Mount Charles Formation* Basalt and basalt breccia interbedded with turbidites; low-K tholeiite chemistry; interpreted as continental flood basalt; ?1,800–?1,790 Ma *Frederick Suite* Magnetic, peraluminous biotite monzogranite to syenogranite with hornblende in SiO_2-poorer samples; age ranges from ~1,815 to 1,790 Ma; inferred to have deeper source *Grimwade Suite* Non-magnetic, peraluminous biotite monzogranite to syenogranite with hornblende in SiO_2-poorer samples; age ranges from ~1,820 to 1,790 Ma; inferred to have shallower source	D_5 Shear zones, thrusts and oblique-slip faults; important locus of mineralization through Tanami region. Most gold introduced during this event D_4 ESE-trending crenulations; angular folding late syn- to post-granite intrusion *Post-*D_3 Extension and deposition of Mt. Charles Formation in continental rift; ?1,800–?1,790 Ma D_3 Open, angular NNW- to NE-trending folds with wavelengths of 0.5–50 m (mesofolds) and 5–10 km (macrofolds); ?1,810–?1,800 Ma (may correlate with Stafford Event in Arunta) D_2 NE- to E-trending chevron folds with 100 m wavelength; ?1,810–?1,800 Ma
1,825–1,815	Ware Group *Wilson Formation* Graywacke, quartz wacke and siltstone; age constrained between ~1,815 and ~1,802 Ma *Century Formation* Conglomeratic sandstone, siltstone and fine-grained sandstone; age inferred at 1,825–1,815 Ma from regional relationships *Nanny Goat Volcanics* Volcanogenic sandstone interbedded mainly with felsic volcanic rocks; age ~1,820 from associated volcanic units	*Birthday Suite* Felsic volcanic rocks of the Ware Group and the Winnecke Granophyre; also includes monzogranite and granodiorite; highly magnetic; restricted to northeastern part of Tanami region	

1,835–1,825	*Mt. Winnecke Formation* Coarse-grained quartz sandstone and granular conglomerate; ~1,825 Ma based on interbedded rhyolite		*Tanami Event (D_1)* Asymmetric, disharmonic folds with wavelengths to 1 km; greenschist to mid-amphibolite facies metamorphism with highest grades to southeast. Introduction of some gold?
~1,840	Tanami Group	*Dolerite sills* Intruded Dead Bullock Soak and Killi Killi Formations; peperitic textures locally developed	
	Killi Killi Formation Turbiditic sandstone and siltstone; maximum depositional age ~1,840 Ma *Dead Bullock Formation* Siltstone and sandstone (Ferdie Member: ~1,838 Ma) fining into graphitic siltstone and BIF (Callie Member)		
~1,865	*Bald Hill sequence* Turbiditic sandstone and siltstone	*Basalt and dolerite sills* Basalt interbedded with turbidites *Felsic sill* High-level quartz porphyry associated with dolerite sills	
~1,880			*Barramundi Orogeny* Upper amphibolite facies metamorphism affecting Billabong Complex
~2,510	*Billabong Complex* Meta-arkose	*Billabong Complex* Leucogranite	

harmonic folding with wavelengths of macrofolds of ~1 km and regional greenschist to amphibolite facies metamorphism. The Tanami Event was followed by deposition of sandstone, siltstone, and felsic volcanic rocks of the ~1,820–Ma Ware Group. The Ware Group was accompanied by the intrusion of the high-level Winnecke Granophyre. These volcanic and intrusive rocks comprise the Birthday magmatic suite.

Between 1,820 and 1,790 Ma, the Tanami region experienced a complicated history involving two periods of compressional deformation (D_2 and D_3), the development of a post-D_3 rift filled with turbiditic sedimentary rocks and basalt of the Mount Charles Formation, the intrusion of the Grimwade and Frederick magmatic suites, and N–S directed (D_4) and WSW–ENE-directed (D_5) shortening (Crispe et al. 2006). Most of the lode–gold deposits in the Tanami region are associated with D_5 shear zones and fault systems. It is possible that some or all of these events are related to progressive deformation, but data to test this hypothesis were not available at the time of writing.

Seismic data (Goleby et al. 2006) and inversion and forward modeling of potential field data (Vandenberg and Meixner 2003; Meixner and Lane 2005) indicate that granite complexes at the surface have high aspect ratios and maximum thicknesses of 5–7 km. The same data preclude the existence of large granite bodies deeper in the crust.

The grade of metamorphism tends to increase from northwest to southeast (Vandenberg et al. 2001; Fig. 3), with gold deposits known in all metamorphic facies. Although the highest-grade metamorphism occurred during the Tanami Event (Scrimgeour and Sandiford 1993; Vandenberg et al. 2001), contact aureoles commonly develop around granites (Fig. 3). These thermal aureoles, which are characterized by hornfels and the growth of metamorphic minerals such as andalusite (chiastolite), almandine, cordierite and biotite, extend up to 5 km (mostly tens to hundreds of meters) away from granitoid contacts at surface (Fig. 3; Tunks 1996; Wygralak et al. 2005; Crispe et al. 2006).

The older stratigraphic units are overlain by the Pargee Sandstone, which itself is unconformably overlain by sandstone, siltstone, shale, and carbonate of the Birrindudu Group. The age of the Pargee Sandstone is constrained by a 1,758±15-Ma maximum depositional age (Cross and Crispe 2006) and a 1,632±3-Ma age of xenotime associated with epigenetic REE–Th–U mineralization (Vallini et al. 2006).

Late brittle faults (D_{6+}), including the WNW-trending Tanami and Mongrel Faults cut all units in the Tanami region. A number of zircon U–Pb discordia in samples from the western Tanami yield lower intercepts at 550–600 Ma (D. Maidment, unpublished data), indicating a thermal

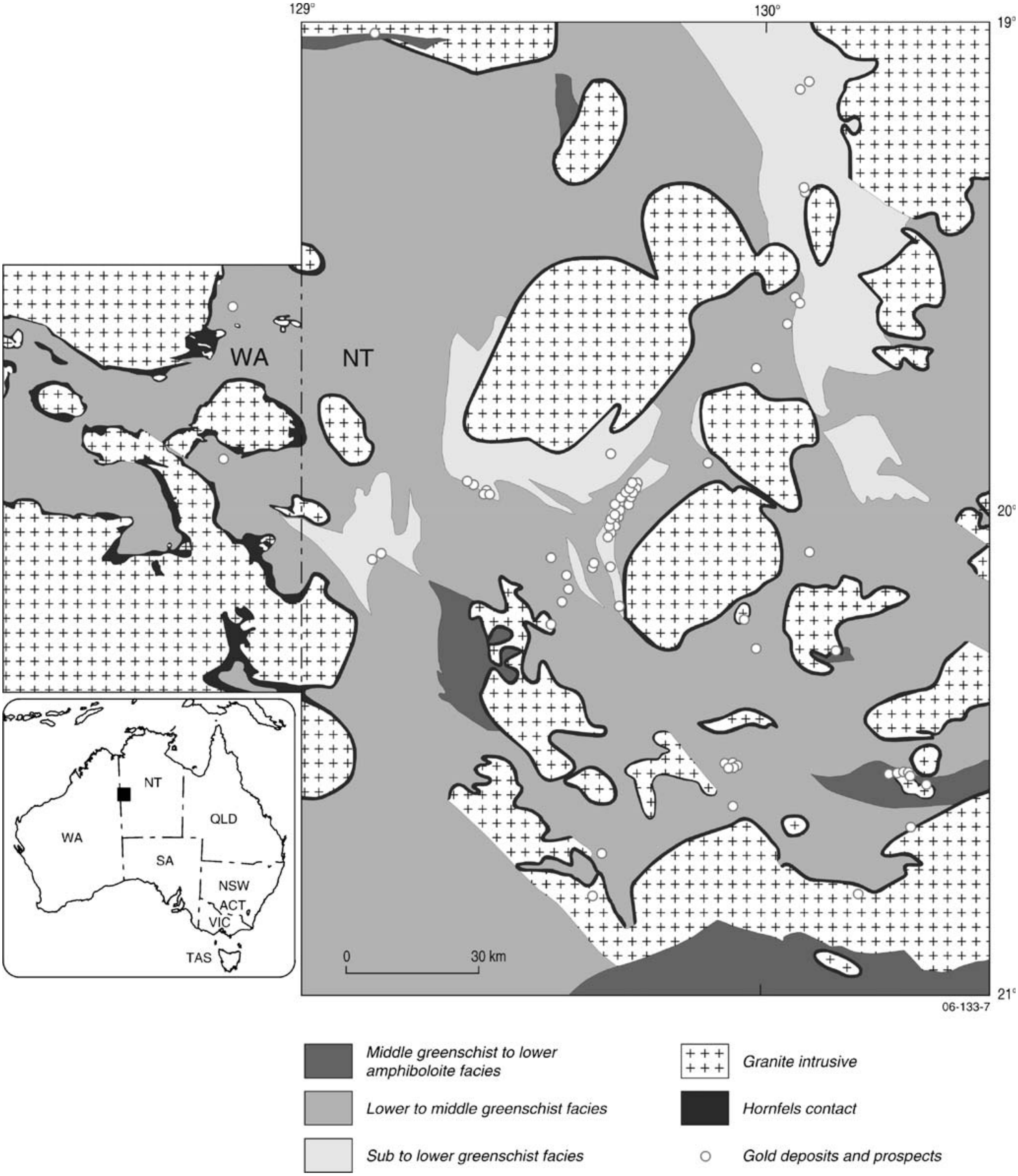

Fig. 3 Metamorphic facies map of the Tanami region

event at this time. This age corresponds to the King Leopold Orogeny in the Halls Creek region and Kimberley Craton (Blake et al. 2000). Faults associated with this orogeny have a similar orientation and offset to the Tanami and Mongrel Faults (Fig. 2), suggesting a King Leopold age to some D_{6+} structures, although the age of other D_{6+} structures may be as young as the Alice Springs Orogeny (450–300 Ma; c.f. Haines et al. 2001).

Mineral deposits of the Tanami region

Like the Yilgarn and Superior cratons and many other lode–gold provinces (Hodgson 1993), gold is hosted by a variety of rock types. However, unlike many of these provinces, the majority of gold in the Tanami region is hosted by sedimentary rocks (including iron formation), with mafic rocks (basalt and dolerite) as the other significant host. Table 2 summarizes the characteristics of these deposits and other significant prospects. Figure 4 shows the relative importance of various host rocks to gold mineralization.

Deposits hosted mainly by sedimentary rocks

Two of the three major goldfields within the Tanami region, The Granites and Dead Bullock Soak, are hosted exclusively by carbonaceous or iron-rich sedimentary units. Other isolated deposits, including Oberon, Coyote, and Minotaur, are also hosted by sedimentary rocks. In total, these deposits comprise 77% of the Tanami gold resource, with carbonaceous sedimentary rocks containing 61% and banded iron formation containing 16% (Fig. 4).

Deposits hosted by carbonaceous rocks

Fine-grained, clastic, carbonaceous, sedimentary units in the Dead Bullock Soak and Killi Killi Formations are the most important host of gold in the Tanami region. The most significant deposit of this type is the Callie deposit (Fig. 5), which has a total resource of 188 tonnes of gold (Table 2). This deposit is localized within carbonaceous siltstone where D_5 structural corridors intersect anticlinal closures in the D_1 Dead Bullock Soak Anticlinorium (Smith et al. 1998; Voulgaris and Emslie 2004: Fig. 5a,b). As a consequence, the ore shoots have a regular plunge of about 45° to the east. Although stratabound in general character, the mineralized zone transgresses up stratigraphy down plunge. The host sequence, which is characterized by carbonaceous siltstone, includes a distinctive unit up to 22 m thick termed the Callie Boudin Chert (Williams 2006). This unit, which is characterized by chert "boudins" up to 3 cm in thickness (Fig. 6a), is interpreted as a nodular chert formed along a maximum flooding surface and the enclosing carbonaceous siltstones as sedimentary rocks formed in a deepwater, sediment-starved distal fan environment (Lambeck 2004).

At Callie, sheeted, planar to weakly boudinaged quartz veins up to 200 mm thick host free gold with variable carbonate, chlorite, biotite, feldspar, and sulfide minerals (Table 2). These veins dip 63° to 160° and define a series of E–W-trending D_5 corridors. Individual corridors can exceed 100 m in width and obliquely cut the D_1 Dead Bullock Soak Anticlinorium (Fig. 5a; Voulgaris and Emslie 2004; Williams 2006).

The most significant effect of ore-related alteration at Callie is pervasive bleaching, which is caused by the destruction of carbonaceous material in the host rocks. Ore veins are generally surrounded by a narrow zone of wall rock alteration that varies with depth, with chlorite being progressively replaced by biotite as the dominant phyllosilicate (Smith et al. 1998). The Ferdies Member, which underlies ex-carbonaceous siltstone of the gold-bearing Callie Member, comprises fine-grained sandstone and siltstone with magnetite content up to 50% (Voulgaris and Emslie 2004; Williams 2006). Many of the sills that punctuate the stratigraphic sequence in the Dead Bullock Soak goldfield are extensively carbonated.

Although not as well-studied, the Oberon prospect shares many characteristics with the Callie deposit. It is hosted by carbonaceous siltstone within the Killi Killi Formation, and a significant proportion of the mineralized rock is hosted within the axial zone of a preexisting (D_2) anticline (Wygralak et al. 2005). The vein paragenesis is similar to Callie, with gold hosted by quartz–K–feldspar–carbonate–pyrite veins with chlorite-bearing wall rock alteration zones. The Oberon prospect is also characterized by pervasive decarbonization and bleaching of the host rock (Table 2; Wygralak et al. 2005).

The other important deposit hosted by clastic sedimentary rocks is the Coyote deposit. Mineralization within this deposit is hosted mainly along the sheared south limb of a D_1 anticline (Fig. 7a). Ore lenses, which consist of quartz vein arrays, plunge 10–15° to the west. Although the Coyote ore shoots are hosted by a turbiditic sandstone-dominated package, in detail, most veins occur within siltstone interbeds (Bagas et al. 2006).

In the nearby Bald Hill area (Bagas et al. 2006), a number of prospects are localized within the folded Bald Hill sequence. This sequence, although N-trending, is folded by a series of WSW-plunging folds (Fig. 7b), with mineralization related to E- to SE-trending faults. Timing of auriferous veins relative to structural elements indicates a pre- to syn-D_1 timing for these prospects.

The smallest deposit hosted by clastic sedimentary rocks is the Tregony deposit, which is hosted by graywacke and shale of the Killi Killi Formation. This prospect differs from the other deposits in that it is hosted by N-striking veins in NW-trending dilational jogs related to a regional shear zone (Table 2; Wygralak et al. 2005; Ord River Minerals 2005).

Deposits hosted by iron-rich sedimentary rocks

Iron-rich sedimentary rocks near the stratigraphic top of the Dead Bullock Formation host mineralization in the Dead Bullock Soak (Figs. 3c and 5a) and The Granites (Fig. 8)

Table 2 Characteristics of important lode-gold deposits and prospects in the Tanami region

Deposit	Production and remaining resource[a]	Host rock and stratigraphic context[b]	Structural context[b]	Vein paragenesis and alteration	Ore fluid characteristics	Data source(s)
Deposits hosted mainly by graphitic sedimentary rocks and banded iron formation						
Dead Bullock Soak goldfield						
Dead Bullock Ridge, Triumph Hill, Colliwobble Ridge and Sleepy Hollow	Production, 1.26 Mt @ 3.9 g/t; resource, 3.05 @3.4 g/t; total, 16.4 t (0.496 MOz)	The ores are mainly hosted by the Schist Hills iron member (SHIM) in the Callie Member. The SHIM consists of interlayered amphibole–chlorite–magnetite rock and chert. Highest grade is adjacent to dolerite sills. Although the deposit overall is stratabound, individual ore shoots cut stratigraphy.	The ores occur in the F_1 Dead Bullock Soak anticlinorium, with the richest zones in parasitic folds or structural thickened zones. The orebodies are complexly dislocated by D_6 faults. At Triumph Hill, the best grade is at intersection of D_5 faults with SHIM.	Two vein sets are present: (1) deformed chlorite veins and (2) late buck quartz veins. Visible gold is associated with the chlorite veins, which also contain arsenopyrite, or in the wall rocks to the veins, where it is associated with abundant pyrite and arsenopyrite. In contrast to the Villa deposit (below), the majority of the gold is hosted by the chlorite veins. Alteration includes: (1) early chlorite–carbonate alteration of dolerite, (2) post-ore (?) biotite alteration, (3) post-ore amphibole alteration in iron-rich units, and (4) post-ore sericite–carbonate–pyrite alteration.	N/A	Smith et al. (1998), Wygralak et al. (2005) and references therein
Villa, Fumerole and Avon	Resource, 3.33 Mt @ 3.6 g/t; total, 11.9 t (0.382 MOz)	Stratabound ores are hosted mainly in iron-rich sediment rocks ("Orac formation") in the Callie Member. Ore is also present in adjacent pelitic rocks. The iron-rich units are chlorite-rich with chert bands, amphibole–pyrite-rich layers and local massive carbonate.	The ores occur in the F_1 Dead Bullock Soak anticlinorium, with the richest ore shoots developed in zones of greatest deformation such as anticlinal fold closures and parasitic flexures on fold limbs.	Three vein sets are present: (1) pre-ore, bedding parallel quartz veins, (2) D_5 sheeted quartz veins, and (3) late buck quartz veins. However, gold is mainly associated with arsenopyrite and pyrrhotite disseminated within the iron-rich units. Gold is present to a lesser extent in sulfide-poor amphibole-rich rocks and in chloritic bands in (D_5?) quartz veins. Massive carbonate layers are replaced by amphibole. Potassium metasomatism in inferred to have formed biotite porphyroblasts within pelitic rocks.	N/A	Smith et al. (1998), Wygralak et al. (2005) and references therein
Callie	Production, 10.0 Mt @ 5.3 g/t; resource, 22.0 Mt @ 6.1 g/t; total 188 t (6.03 MOz)	The ores are hosted by carbonaceous siltstone of the Callie Member. The orebodies obliquely transgress stratigraphy: ores in the deeper levels of the deposit are localized at higher stratigraphic levels.	Gold-bearing veins are hosted by D_5 structural corridors that obliquely cut the F_1 Dead Bullock Soak anticlinorium. Orebodies are best developed where the structural corridor cuts the nose or northern limbs of parasitic anticlines within the anticlinorium. The gold veins dip 63° to 160°.	Four vein sets are present: (1) pre-ore, bedding-parallel quartz veins with minor chlorite and pyrite; (2) syn-ore (D_5), planar quartz veins with variable chlorite, biotite, apatite, carbonate, feldspar, pyrite, pyrrhotite, chalcopyrite, gold, ilmenite, arsenopyrite, marcasite and anatase; (3) post-ore carbonate–quartz veins	T_h, 254–326°C; salinity, 4–7 eq wt% NaCl; gases: CO_2:N_2: CH_4= 0.81:0.17:0.02; phase separation indicated; depth, 2.6–5.0 km; $\delta^{18}O$, 5.5±1.6‰	Smith et al. (1998), Wygralak et al. (2005) and references therein, Voulgaris and Emslie (2004), Mernagh and Wygralak (2006), Williams (2006)

				with accessory sphalerite, galena and pyrite; and (4) late carbonate veins. Ore-related alteration includes: (1) total decarbonization of host, (2) wall-rock assemblages changing from carbonate ± chlorite ± quartz ± pyrite to chlorite ± titanite ± rutile and biotite ± ilmenite ± epidote ± pyrrhotite with depth, and (3) magnetite growth within well-bedded units underlying the ore host.		
The Granites goldfield						
Bullakitchie, Shoe, Quorn and Bunkers Hill	Production, 4.6 Mt @ 4.58 g/t; stockpile, 4.0 Mt @ 1.5 g/t; resource, 0.63 Mt @ 3.3 g/t; Total 29.2 t (0.937 MOz)	Iron-rich metasediment rocks in the Callie Member host ores. The host, mainly amphibole ± garnet rock with variable magnetite, occurs in a pelitic to psammitic sequence, which is graphite-bearing above but graphite-free below the host. Calcite–dolomite rock with accessory quartz, diopside and grossular, is developed in the host unit at East Bullatkitchie.	Gold is closely associated with D_1 layer-parallel shears and, to a lesser extent, with shears reactivated during D_5 folding. The orebodies dip steeply (70–90°) and range in strike from east to NE.	Four main vein sets are present: (1) boudinaged calc-silicate veins that are cut by other vein sets; (2) folded quartz ± carbonate shear and extensional veins (syn-D_1) with minor pyrrhotite, arsenopyrite, and loellingite; (3) quartz, quartz–carbonate, and calcite shear veins (syn-D_3) with minor pyrrhotite; and (4) tensional quartz–calcite veins (syn-D_4). Gold is associated mainly with sets 2 and 3, particularly shear veins in set 2. Disseminated sulfide (<5%; mostly pyrrhotite, pyrite and arsenopyrite) in the host formed during D_1 and D_5. Loellingite formed during D_1, but not D_5. Narrow wall rock alteration zones form around most veins. Quartz veins have a hornblende ± cummintonite ± epidote assemblage, whereas calcite veins have a diopside–clinozoisite assemblage.	T_h, 240–312°C; salinity, 0–14 eq wt% NaCl; gases: CO_2:N_2:CH_4= 0.81:0.16:0.03; phase separation indicated; depth, 3.0–9.8 km; $\delta^{18}O$, 3.8±1.8‰	Mayer (1990), Adams (1997), Wygralak et al. (2005), Adams et al. (2006), Mernagh and Wygralak (2006). Structural chronology follows Table 1.
Other deposits						
Oberon	Resource, 4.45 Mt @ 2.9 g/t; total, 12.9 t (0.415 MOz)	The ores are hosted by graywacke and siltstone with fine graphitic and pyritic interbeds of the Killi Killi Formation. Foliated dolerite sills intrude the host rock. Ores occur preferentially in fine decarbonized sedimentary rocks.	The orebodies are associated with an isoclinal D_2 anticline. Two lodes are present: a north lode in the axial zone of the anticline and a south lode in the southern limb.	Three vein sets are present: (1) D_1, boudinaged quartz vein with K–feldspar, pyrite, and scattered gold; (2) syn-ore (D_5), planar quartz–K–feldspar–carbonate–pyrite veins with wall rock arsenopyrite; and (3) late (D_6) carbonate veins with minor pyrite. Ore is spatially associated with decarbonization and pervasive sericitic alteration of siltstone. Alteration directly associated with	N/A	Wygralak et al. (2005) and this study

Table 2 (continued)

Deposit	Production and remaining resource[a]	Host rock and stratigraphic context[b]	Structural context[b]	Vein paragenesis and alteration	Ore fluid characteristics	Data source(s)
				veins is quartz ± carbonate ± feldspar ± chlorite.		
Minotaur	Resource, 0.67 Mt @ 3.06 g/t; total, 2.05 t (0.066 MOz)	Metasedimentary rocks of the Callie Member host ore. Iron-rich amphibole–quartz rocks that host ore correlate with the Main Host Unit at The Granites. Dolerite sills and flat-lying felsic bodies intrude the host sequence.	The host is affected by isoclinal D_3 folds, and by open D_4 and D_5 folds. The orebody lies on the west side of the D_4 Minotaur Anticline, but the relationship of ore to structure is unclear.	Gold occurs in fine chloritic fractures/veinlets and associated with sulfides (arsenopyrite and pyrrhotite) in the host unit. Gold also occurs in quartz–feldspar ± chlorite veins in metasedimentary rocks stratigraphically underlying the host unit.	N/A	Wygralak et al. (2005)
Coyote	Resource, 2.66 Mt @ 5.24 g/t; total, 13.9 t (0.447 MOz)	Ore shoots are hosted by Killi Killi Formation, mostly in silstone/shale interbeds within graywacke-dominated sequence.	10–15° west-plunging ore lenses adjacent to shear along the steeply dipping south limb of west-plunging F1 anticline. Gold is hosted by bedding-parallel quartz veins.	Gold occurs in the last paragenetic stage of D_5 quartz veins in association with arsenopyrite, calcite, K–feldspar, biotite (altered to chlorite), pyrite, galena, sphalerite, chalcopyrite, and bismuth minerals. This assemblage fills the centers of veins or tensional fractures that cut these veins. The host rocks are commonly biotite (chlorite) altered within a few millimeters of auriferous veins. Other alteration assemblages, including include quartz–sericite–pyrite–chlorite, silica–dolomite, quartz–K–feldspar, graphite, and chlorite ± biotite, are also present but not related to gold.	T_h, 290–360°C; salinity: 0–7 eq wt% NaCl; gases: CO_2:N_2:CH_4= 0.82:0.06:0.09 (CO_2-rich); 0.01:0.08:0.91 (CH_4-rich); phase separation indicated; depth, 3.4–7.5 km	Bagas et al. (2006) and Mernagh and Wygralak (2006)
Bald Hill (includes Kookaburra and Sandpiper)	Resource: Kookaburra: 1.44 Mt @ 2.02 g/t, total: 2.91 t (0.094 MOz) Sandpiper: 1.21 Mt @ 2.92 g/t, total: 3.53 t (0.114 MOz)	The deposits are hosted by carbonaceous siltstone of Bald Hill sequence (interlayered basalt and siltstone) in Killi Killi Formation.	Auriferous veins occur where east-trending shears cut the Bald Hill sequence.	Gld is associated with syn- to late D_1 quartz–carbonate quartz ± pyrite ± arsenopyrite veins with variable amounts of sericite, K–feldspar and marcasite, and minor to trace quantities of biotite, amphibole, apatite, sphalerite, and pyrrhotite. Galena is also present in carbonate veins with a similar structural timing. The auriferous veins are associated with sericite–quartz ± biotite ± sulfide schist, which is interpreted as an alteration assemblage. Sulfides in this schist include arsenopyrite, pyrite, galena, chalcopyrite, sphalerite and altaite.		Hassan (2002) and Bagas et al. (2006)
Tregony	Resource, 1.098 Mt @ 1.57 g/t; total, 0.63 t (0.055 MOz)	Graywacke and shale of the Killi Killi Formation host the prospect.	Gold is in N-trending veins hosted by NW-trending dilational jogs in the Supplejack Fault Zone.	Gold forms part of a mineralized assemblage including quartz, chlorite, pyrite, and arsenopyrite.	N/A	Wygralak et al. (2005), Ord River Minerals Prospectus, Ord River Minerals (2005)

Deposits hosted mainly by mafic igneous rocks						
Tanami goldfield						
Tanami mine corridor	Production, 11.46 Mt @ 2.40 g/t; resource, 7.19 Mt @ 3.2 g/t; total, 50.6 t (1.63 MOz)	The Tanami mine corridor hosts more than 40 deposits over a 15-km long NNE-trending zone within the Mount Charles Formation. Similar deposits are present further to the south in the Jims Find and Pendragon areas. Basalt is the main host to the ores. However, ore is also present in the base of carbonaceous mudstone units above basalt flows.	Four brittle fault generations are present: (1) pre-ore growth faults; (2) pre-ore low angle thrusts (early D_5); (3) syn-ore (D_5) wrench faults with small displacement; and (4) post-ore, sub-vertical and bedding-parallel faults (D_6). Auriferous vein sets and ore shoots have three main trends: 350–000°, 020–040°, and 060–070°. These veins dip moderately to steeply to the south and east.	Six vein sets are present: (1) dolomite–hematite–sericite ± quartz veins in extensional faults; (2) early ore quartz ± sericite ± pyrite veins; (3) late ore carbonate–quartz ± chalcopyrite ± chlorite ± gold ± sericite ± chlorite veins; (4) post-ore (D_6) quartz ± pyrite ± chalco-pyrite ± covellite and dolomite ± chlorite ± quartz ± sericite ± hematite veins in bedding-parallel faults; (5) post-ore irregular chlorite-carbonate veins (D_6); and (6) post-ore calcite± chalcopyrite±quartz veins (D_6). Vein set 2 contains chlorite, arsenopyrite, sphalerite, and gold. In vein set 3 gold occurs as inclusions in chalcopyrite. Epithermal-like textures are present in some ore-stage veins. Sericite ± quartz ± pyrite ± carbonate ± chalcopyrite-altered zones extend to 10 m from ore zones and to 10 cm about ore-stage veins. A chlorite–carbonate assemblage that overprinted the Tanami mine corridor may be the outer zone of mineralization-related alteration. Carbonate ± chlorite zones are associated with vein set 5.	T_h, 200–340°C; salinity: 0–21 eq wt% NaCl; gases, rare CO_2; phase separation indicated; depth, 1.5–5.6 km; $\delta^{18}O$, 8.5±2.4‰	Tunks (1996), Tunks and Marsh (1998), Wygralak et al. (2005), Mernagh and Wygralak (2006), Tunks and Cooke (2006)
Other deposits						
Groundrush	Resource, 4.99 Mt @ 4.55 g/t; total, 22.7 t (0.730 MOz)	The ore is hosted by a foliated dolerite dike that intruded Killi Killi Formation graywacke near the chilled margin of the Talbot South Granite.	10 to 30-m wide lodes consist of anastomosing zones of NNE-trending veins that dip 70–80° to the west.	Mineralization is in anastomosing zones of steeply dipping quartz veins and is associated with chloritic alteration. Gold occurs as native gold or is associated with arsenopyrite, pyrite and pyrrhotite. The auriferous veins also contain chalcopyrite and K–feldspar.	T, 260–430°C; salinity, 1–14 eq wt% NaCl; gases: CO_2:N_2:CH_4= 0.45:0.03:0.51; phase separation *not* indicated; depth, 5.6–11 km	Wygralak et al. (2005) and Mernagh and Wygralak (2006)
Crusade	Resource, 1.4 Mt @ 2.4 g/t; total 2.32 t (0.075 MOz)	Mineralized zones are localized along a steeply dipping, faulted contact between dacite and basalt, with most mineralization in the basalt.	The shallow north-plunging ore zone consists of ~20 quartz veins that dip 50–85° to the west at the faulted contact.	Quartz veins with pyrite, arsenopyrite, and gold	N/A	Wygralak et al. (2005)

Table 2 (continued)

Deposit	Production and remaining resource[a]	Host rock and stratigraphic context[b]	Structural context[b]	Vein paragenesis and alteration	Ore fluid characteristics	Data source(s)
Deposits hosted by other rock types						
Galifrey	N/A	The mineralized zone is hosted by tonalite and the Killi Killi Formation.	Mineralized veins are controlled by sinistral (D_5?) shears.	Three vein sets are present: (1) quartz–albite; (2) quartz–carbonate ± pyrite; and (3) quartz–chlorite ± sericite ± pyrite.	N/A	Wygralak et al. (2005)

[a] As of 31 December 1996, for BIF-hosted deposits in Dead Bullock Soak goldfield; 30 June 2001 for the Callie, Oberon, Minotaur and Groundrush deposits; June 2002 for deposits in the Tanami goldfield (including deposits in the Jims Find and Pendragon areas); 31 December 2002 for The Granites goldfield; and 30 January 2004 for the Coyote, Kookaburra and Sandpiper deposits. Resource data for the Crusade and Tregony prospects were calculated in 1996 and 2000, respectively. Data is drawn from the Registry of Australian Mining 2003–2004, from company data releases and from Smith et al. (1998). The last source was used for deposits in the Dead Bullock Soak goldfield (except Callie) as more recent data grouped production from this goldfield with that from The Granites goldfield. Phil Ferenczi (NTGS) and Mike Huleatt (GA) synthesized some data presented.

[b] The structural and stratigraphic nomenclature used herein is that of Crispe et al. (2006). Mine-scale structural and stratigraphic schema (e.g., Smith et al. 1998) have been generalized to fit into this nomenclature.

goldfields and at the Minotaur deposit. These iron-rich rocks comprise chert interlayered with amphibole (hornblende and/or cummingtonite)-rich rock with variable amounts of chlorite, magnetite and, at The Granites, garnet (Table 2; Mayer 1990; Smith et al. 1998; Wygralak et al. 2005). Massive carbonate is locally preserved at The Granites goldfields and at the Villa deposit in the Dead Bullock Soak goldfield, leading to the interpretation that these iron-rich rocks are metasomatized sulfide, carbonate, or silicate facies banded iron formation (BIF; Mayer 1990; Smith et al. 1998). The BIF host rocks occur in pelitic to semipelitic sequences that are locally mineralized adjacent to some deposits. In The Granites goldfield, the surrounding rocks are decarbonized below the ore host, but graphitic above (Mayer 1990).

In the Dead Bullock Soak goldfield, the highest gold grades in BIF-hosted deposits are in parasitic folds, particularly anticlinal fold closures, in the D_1 Dead Bullock Soak Anticlinorium (Figs. 3c and 5a; Table 2; Smith et al. 1998). This contrasts with deposits in The Granites goldfield, where ore lenses have a tabular form (Fig. 8b), are not localized in fold closures and are controlled by layer-parallel shears (Adams et al. 2006).

Structural relationships highlighted by Mayer (1990), Adams (1997), and Adams et al. (2006) suggest that some gold was introduced early (during D_1) in The Granites goldfield, with a secondary period of gold mineralization during their D_3 (equivalent to D_5). Adams (1997) indicate that most gold-related pyrrhotite, arsenopyrite, and pyrite was developed and flattened within the S_1 fabric, indicating a pre- to syn-D_1 timing of sulfide and gold mineralization. Moreover, Scrimgeour and Sandiford (1993) indicate that alteration selvages around auriferous veins were metamorphosed during emplacement of ~1,795 Ma granites and suggest gold veins were boudinaged during D_1/M_1 granite. However, Vandenberg et al. (2001) interpret that all gold was introduced during D_5. Insufficient data exist to resolve this conundrum.

In addition to quartz-only veins, gold also occurs in chlorite bands within quartz–chlorite veins and as grains associated with sulfide and arsenide minerals disseminated in BIF (Table 2; Mayer 1990; Smith et al. 1998; Wygralak et al. 2005). In The Granites goldfield, the highest tenor gold is associated with sulfide-rich amphibole schist and with carbonate-rich facies BIF. Although the host rock as a whole contains less than 5% sulfide, the amphibole schist typically contains 7–15% sulfide, predominately pyrrhotite, pyrite, and arsenopyrite (Mayer 1990). Even though the BIF-hosted deposits in the Dead Bullock Soak goldfield are not as sulfide-rich, Smith et al. (1998) noted a close association between gold and arsenopyrite abundance in the host rock.

The Minotaur deposit (location to east of Fig. 2) is hosted by iron formation correlated with the host unit in

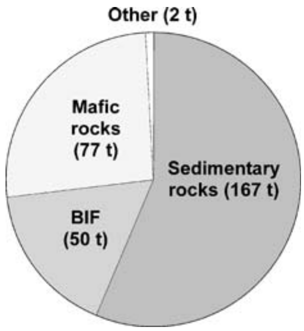

Fig. 4 Pie diagram showing relative contribution to global gold endowment of the Tanami region by host rock

The Granites goldfield. Gold mostly is present in chloritic fractures and is associated with arsenopyrite and pyrrhotite. It also is present in quartz–feldspar veins in metasedimentary rocks underlying the host unit. Although the deposit is associated with a D_3 anticline, detailed structural relationships are unclear (Wygralak et al. 2005).

Deposits hosted mainly by mafic igneous rocks

Mafic igneous rocks are the third major host to gold in the Tanami region, accounting for up to 23% of total gold resources (Fig. 4). Of this 23%, the bulk (14% of the grand total) is from the Tanami goldfield, with the Groundrush deposit contributing a further 6%, and the small Crusade deposit contributing the rest (Table 2). Although mafic igneous rocks contain most of the gold, other rock types, including clastic sedimentary rock and dacite (Table 2), host significant gold in some of these deposits.

The Tanami goldfield

The Tanami goldfield (Fig. 9) differs in many ways from other gold deposits in the Tanami region. This goldfield consists of over 40 individual deposits in a 15-km long zone within the Mount Charles Formation (Fig. 2). This unit, which has a poorly constrained age of 1,800–1,790 Ma, is interpreted to have formed in a post-D_3 continental rift (Tables 1 and 2; Tunks and Marsh 1998; Vandenberg et al. 2001; Wygralak et al. 2005; Tunks and Cooke 2006; Crispe et al. 2006). The Pendragon area, 40 km west, contains similar deposits. The hosts to the deposits underwent, at most, pumpellyite–prehnite metamorphism.

The average deposit in the Tanami goldfield contained less than 1.3 tonnes of gold, and only a handful contained more than 3.0 tonnes. Of these, the largest was the Hurricane-Repulse deposit, which contained 13 tonnes, or slightly more than 25% of the Tanami goldfield total (Wygralak et al. 2005). The three orebodies within this deposit (Fig. 9b) illustrate many of the characteristics of the Tanami goldfield as a whole.

The Hurricane-Repulse deposit consists of auriferous quartz veins and stockworks that were hosted by interbedded basalt, siltstone, and sandstone, with the Repulse (northern) and Gap (central) orebodies hosted by basalt. The Repulse orebody is hosted by brecciated basalt where it is cut by a steeply NNE-dipping D_5 fault near the upper contact with sedimentary rocks. The Gap orebody is located where east-dipping D_5 faults intersect basalt (Wygralak et al. 2005). The siting of ore shoots at the intersection of D_5 structures with basalt is typical of most deposits in the Tanami goldfield. These structures and their associated orebodies have three discrete orientations (350–000°, 020–040°, and 060–070°), all dipping moderately to steeply to the east and southeast (Tunks and Marsh 1998). These D_5 structures include both reverse and small displacement wrench faults (Tunks 1996; Vandenberg et al. 2001; Wygralak et al. 2005).

The southern Hurricane orebody differs from most others in the Hurricane-Repulse deposit and the Tanami goldfield in that it is hosted by sedimentary rock. This orebody is localized where a gently E-dipping fault system intersects sedimentary rocks dipping moderately to the northwest (Fig. 9b: Wygralak et al. 2005), forming three sub-horizontal lenses hosted by siltstone. Erratic, high-grade zones are present at the base of the host unit, just above the underlying basalt. High-grade (to 23% Cu) chalcopyrite-rich zones are locally present in the Hurricane orebody, but appear to cross-cut gold-bearing veins.

Tunks (1996) described a very complex alteration and vein paragenesis (Table 2), which is typical of the parageneses of Tanami goldfield deposits. Significant gold mineralization is restricted to quartz ± sericite and carbonate-quartz veins and breccias associated with D_5 faults. The veins also contain variable pyrite, chalcopyrite, chlorite, and feldspar, and are locally characterized by epithermal-like textures, including comb, colloform, lattice blade, ghost sphere, and flamboyant textures (Adams 1920) as well as chalcedonic quartz (Fig. 6b,c; Wygralak et al. 2005).

Tunks (1996) described pervasive chlorite–carbonate alteration assemblages through the Tanami goldfield, which he interpreted as the outer assemblage associated with gold mineralization. A sericite–quartz ± pyrite ± carbonate assemblage affects the vein host rock up to 1 m from individual veins and 10 m from stockworks.

The Groundrush deposit

The Groundrush deposit is hosted by a thick, foliated dolerite dike that intruded steeply SW-dipping graywacke of the Killi Killi Formation (Fig. 7c). Gold is associated with steeply west-dipping, anastomosing quartz veins that form lodes 10–30 m wide. The dolerite, graywacke, and possibly, the veins are cut by a tonalite dike. The veins are

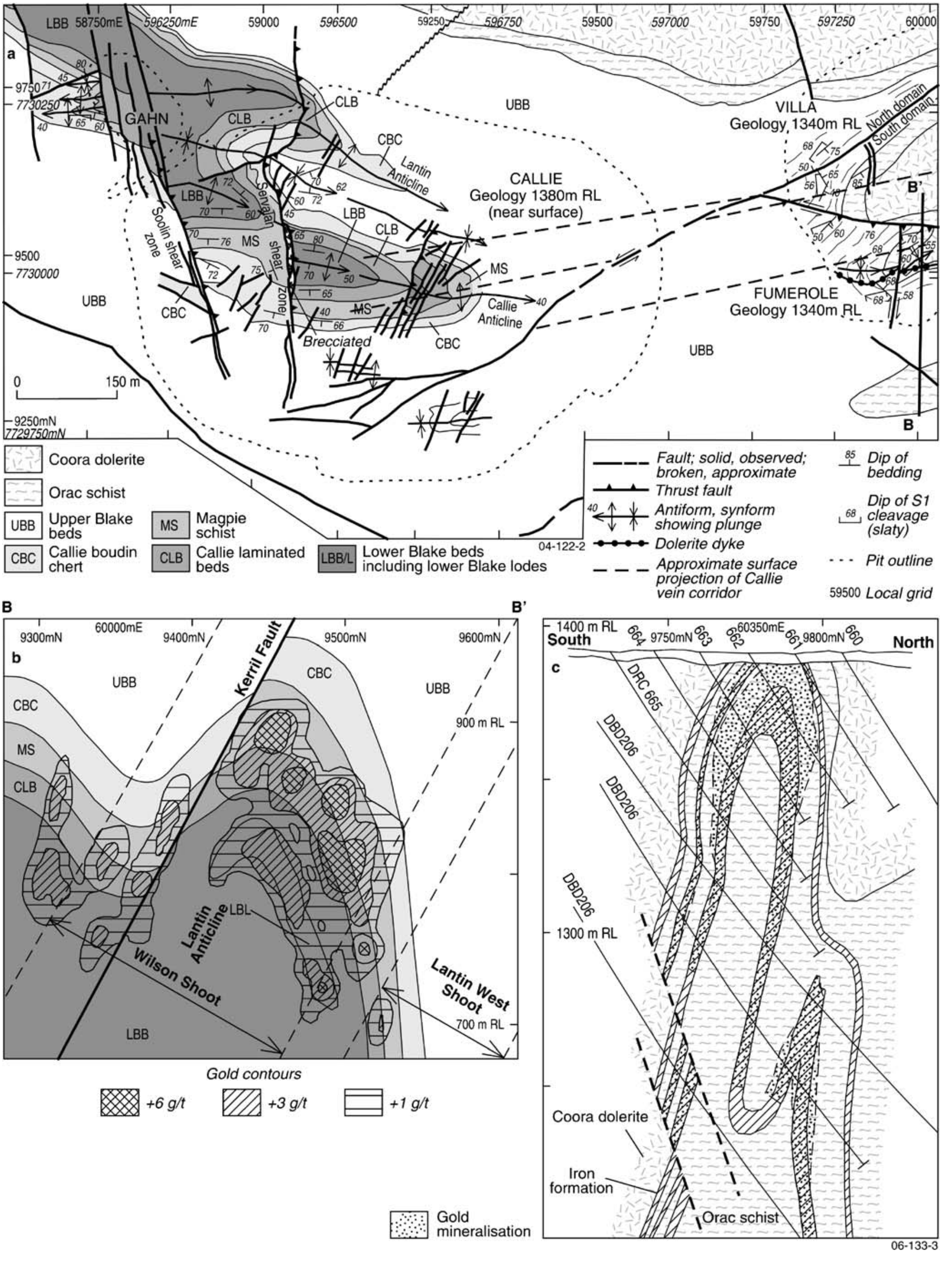
a
LBB
58750mE
596250mE
59000
596500
59250
596750
59500
597000
59750
597250
60000
9750
7730250
9500
7730000
9250mN
7729750mN
GAHN
CLB
CBC
Lantin Anticline
UBB
CALLIE
Geology 1380m RL
(near surface)
VILLA
Geology 1340m RL
North domain
South domain
B'
LBB
MS
Soolin shear zone
Servajan shear zone
Callie Anticline
Brecciated
FUMEROLE
Geology 1340m RL
B
0
150 m
Coora dolerite
Orac schist
Upper Blake beds
Magpie schist
Callie boudin chert
Callie laminated beds
Lower Blake beds including lower Blake lodes
LBB/L
04-122-2
Fault; solid, observed; broken, approximate
Thrust fault
Antiform, synform showing plunge
Dolerite dyke
Approximate surface projection of Callie vein corridor
Dip of bedding
Dip of S1 cleavage (slaty)
Pit outline
59500 Local grid
B
B'
b
9300mN
60000mE
9400mN
9500mN
9600mN
Kerril Fault
UBB
CBC
MS
CLB
900 m RL
LBL
Lantin Anticline
Wilson Shoot
Lantin West Shoot
700 m RL
LBB
Gold contours
+6 g/t
+3 g/t
+1 g/t
1400 m RL
South
664
9750mN
663
60350mE
662
661
9800mN
660
North
c
DRC 665
DBD206
DBD206
DBD206
1300 m RL
Coora dolerite
Iron formation
Orac schist
Gold mineralisation
06-133-3

◀ **Fig. 5** Geology of the Dead Bullock Soak goldfield. **a** Geological plan of goldfield, **b** cross section of Callie deposit (location shown as B–B′ in **a**), and **c** cross section of Villa deposit (located 350 m east of the eastern margin of **c**; modified after Smith et al. 1998; Voulgaris and Emslie 2004)

typically <10 cm wide and contain accessory arsenopyrite, pyrite, pyrrhotite, chalcopyrite, and K–feldspar. Narrow (<2 mm) alteration zones associated with these veins are dominated by sericite. However, the dolerite dike has been chloritized in the lode zones (Wygralak et al. 2005).

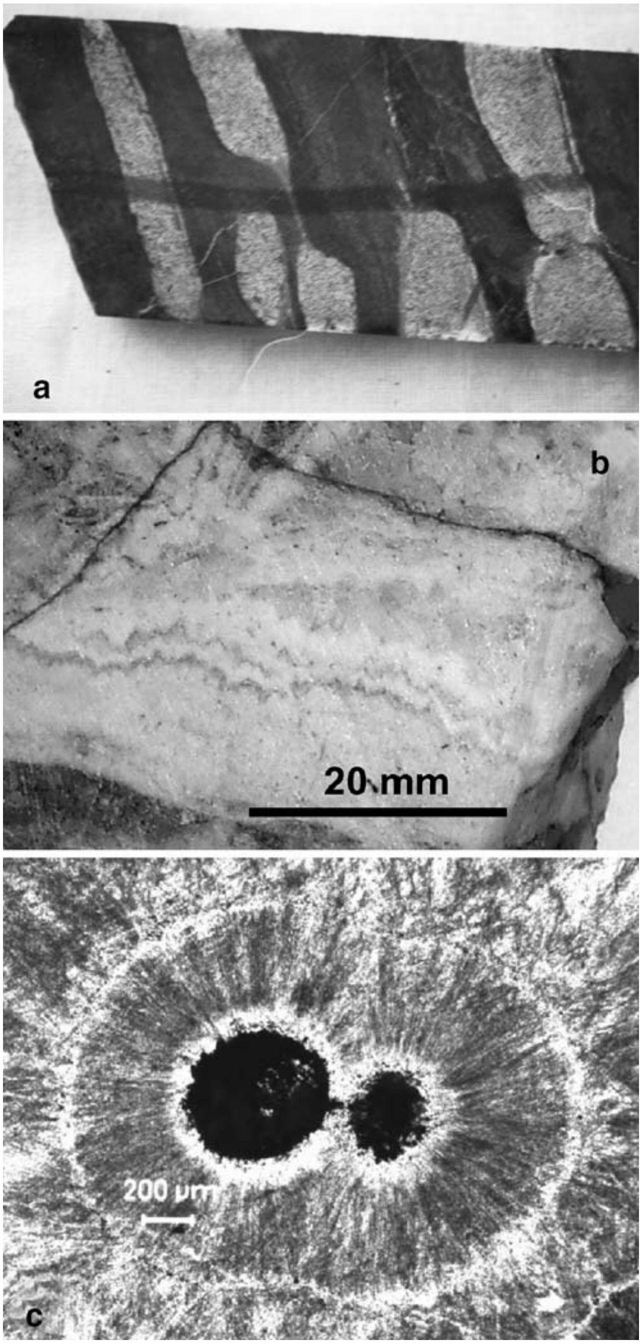

Fig. 6 Photographs of rock textures from the Tanami region. **a** Callie boudin chert, **b** comb-textured quartz from the Tanami goldfield, and **c** photomicrograph of ghost spheres in vein quartz from the Tanami goldfield

Deposits hosted by other rock types

Although resources have not been calculated outside sedimentary and mafic rocks, a few prospects have been identified in other rock types. The most significant of these prospects is the Galifrey prospect (Fig. 2), which is hosted by Grimwade Suite tonalite and graywacke of the Killi Killi Formation. Gold is associated with quartz-carbonate–pyrite veins and stockworks within gently dipping, tensional fractures. The host rocks were pervasively altered to a quartz–sericite–dolomite ± pyrite assemblage (Wygralak et al. 2005). The 1,802±8-Ma Twin Bonanza porphyritic monzogranite also contains gold in thin, quartz-filled fractures (Dean 2001).

The age(s) of mineralization

Like many other gold provinces, the age(s) of mineralization in the Tanami region are poorly constrained, with little robust geochronological data available. Rather, the age of mineralization has generally been inferred based on geological relationships. For instance, some auriferous veins and sulfidic schist at The Granites goldfield (Mayer 1990; Adams 1997) were deformed early (D_1), yet auriferous veins at Callie are planar and inferred to have formed relatively late in the structural history (D_5: Table 2; Smith et al. 1998). Moreover, at The Granites, some gold is also inferred to have been introduced during D_5 (Adams et al. 2006). In the Tanami goldfield, mutually crosscutting relationships between ores and felsic dykes that are compositionally similar to granites in the nearby Frankenia granite complex, suggest a syn-granite age for mineralization (Tunks 1996). Phases of this granite complex have been dated at 1,805±5 Ma (Smith 2001).

Although gold deposition is generally inferred to be coincidental with the deposition of the host quartz veins, in some instances, gold paragenetically fills cracks within the veins. This relationship is best developed at the Coyote deposit (Table 2; Bagas et al. 2006), where it appears to be ubiquitous. Although gold can occur in fractures at the Callie deposit, it is more commonly intergrown with quartz, suggesting coincidental deposition.

With the use of these relationships and the perceived close association of some deposits with granite complexes, genetic models, including syngenetic gold (e.g., Ireland and Mayer 1984) and thermal aureole/granite-related models (Wall and Taylor 1990), have been developed, with implicit ages for mineralization. Howev-

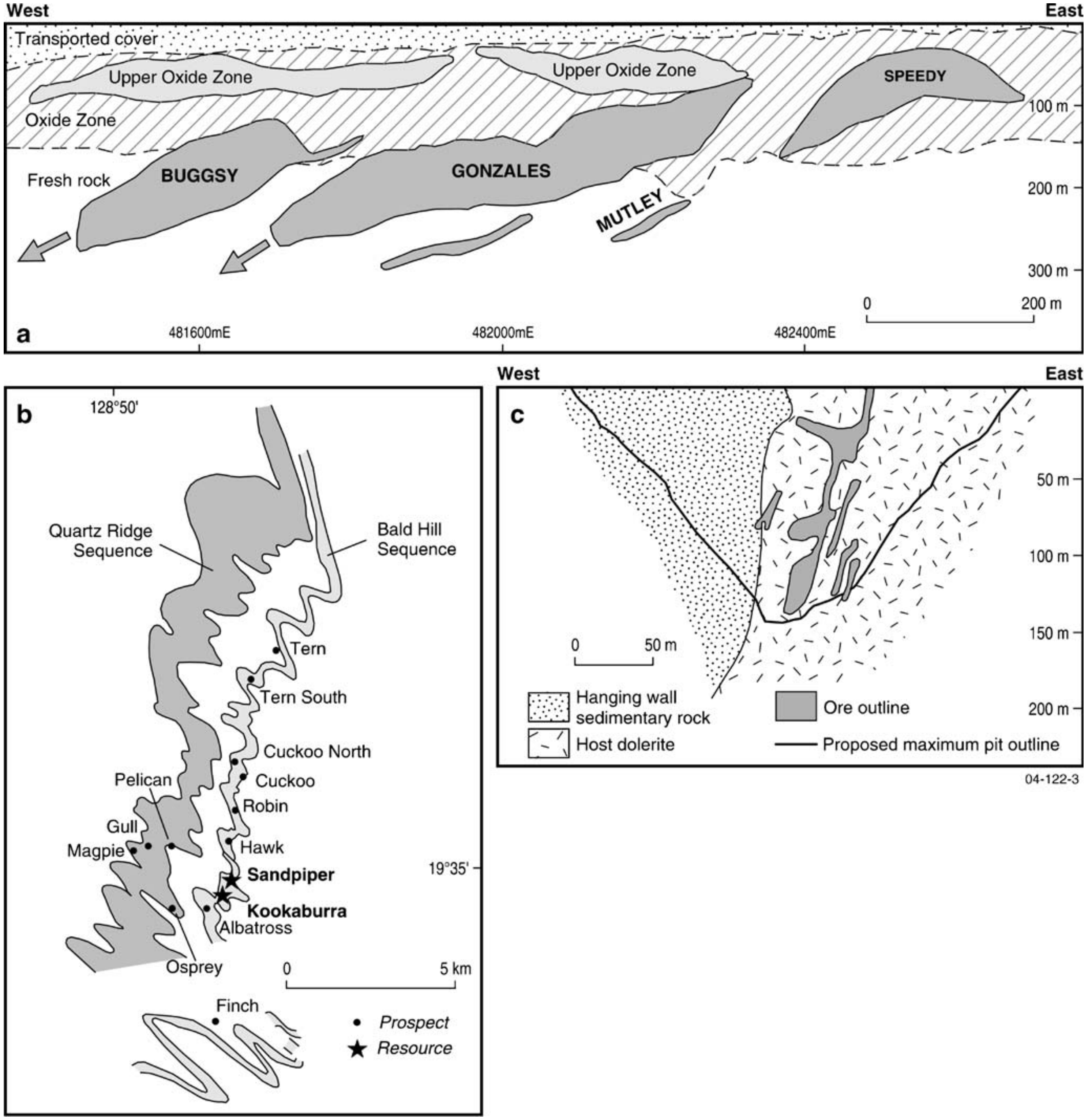

Fig. 7 Geology of selected prospects in the Tanami region. **a** Long section of the Coyote (modified from Tanami Gold NL data), **b** plan showing the association of gold prospects in the Bald Hill area with folds in the Bald Hill Sequence (after Hassan 2002), and **c** cross section of the Groundrush deposit (after Wygralak et al. 2005)

er, until recently, no geochronological data have been collected to test these models. Fraser (2002) suggested that ~1,720 Ma ^{40}Ar/^{39}Ar ages derived from biotite hosted by auriferous quartz veins at Callie reflected the possible age of mineralization. However, preliminary SHRIMP analyses of hydrothermal xenotime paragenetically associated with gold gives ages of 1,803±19 and 1,791±8 Ma at Callie and Coyote, respectively (Cross et al. 2005; Bagas et al. 2006).

Overall, most geochronological data point to an age of around 1,800–1,790 Ma for late (D_5) gold in the Tanami region. The absolute age of the apparently earlier gold event (D_1 at The Granites and in the Bald Hill area) is not constrained.

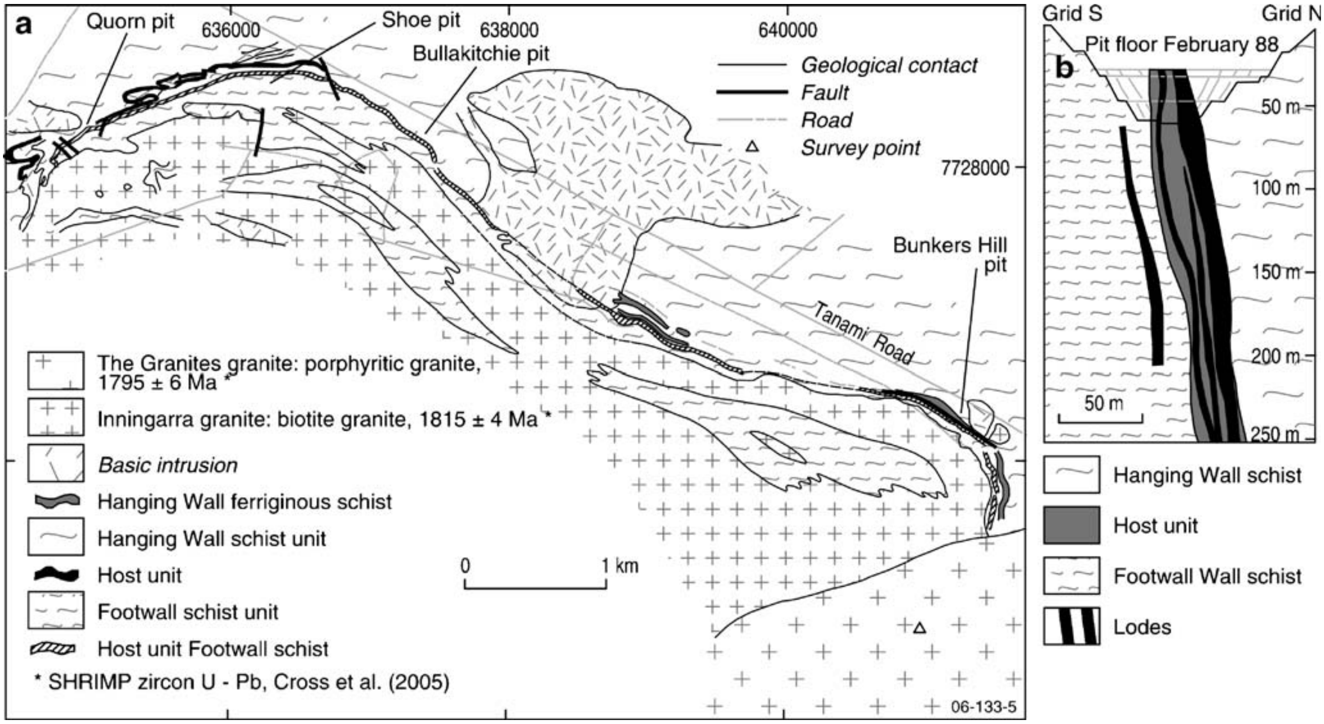

Fig. 8 Geology of The Granites goldfield. **a** Geological plan of the goldfield, and **b** cross section of the East Bullakitchie deposit (modified after Wygralak et al. 2001 and Mayer 1990)

Structural controls on D_5 gold deposits

Figure 2 differentiates faults that formed mainly during D_6 and later deformation events and faults that were active during D_5. The former faults tend to be linear, through-going structures trending WNW to NW, whereas the latter faults tend to be more sinuous, commonly bending into a northerly trend in the northern part of the Tanami region. These latter faults, which include the Bluebush, Supplejack, and Black Peak Fault Zones, are most closely associated with D_5 gold mineralization. The Groundrush deposit and prospects to the north are associated with the Supplejack Fault Zone, deposits in the Tanami goldfield are associated with second- and third-order structures related to the Black Peak Fault Zone, and deposits in the Dead Bullock Soak goldfield are developed along D_5 structural zones.

Figure 10 is a reconstruction of structural elements, granite complexes, and gold deposits at the time of D_5 after removal of strike–slip movement on D_6 structures. The distribution, kinematics, and orientations of the faults were constrained by forward modeling of potential field data (Vandenberg and Meixner 2003), preliminary seismic reflection data (Goleby et al. 2006), and outcrop observations. Strike–dip symbols indicate the trends and dips of quartz veins or ore shoots in major deposits.

Like major D_5 faults, the orientation of the deposits varies systematically with respect to the Coomarie and Frankenia granite complexes. To the northeast of these complexes, the deposits trend northerly, subparallel to the strike of major D_5 faults in the area, whereas to the southeast the deposits trend easterly, at a moderate angle to the major faults (Fig. 10a). Geophysical data indicate that the D_5 structures tap the mid-crust to a depth of at least 10–15 km. However, owing to limited outcrop, the structural regime at the time of mineralization is largely conjectural, and the following discussion must be considered as a working hypothesis.

The D_5 fault system consists of a network of thrust and oblique-slip thrust faults that are consistent with an overall convergent regime with the principal stress direction (σ_1) oriented between ENE–WSW and E–W (Fig. 10b). The Frankenia and Coomarie granite complexes may have acted as buttresses, localizing faults into supracrustal units between or around the complexes.

In the northern part of the Tanami region, deposits parallel the trends of faults, possibly in subordinate thrust-related structures (e.g., ramp-related anticlines). In the south, however, the deposits are mainly oriented ENE to E, at a low to moderateangle to major D_5 structures. The best example of this relationship is at the Callie deposit, where the orientation of tension veins arrays within vein corridors is consistent with ENE-directed shortening, possibly related to local WNW-trending transpressional shear (Fig. 10c).

Tunks and Cooke (2006) proposed that the range in orebody orientations in the Tanami goldfield relate to Reidel geometry developed in a local SE-directed compres-

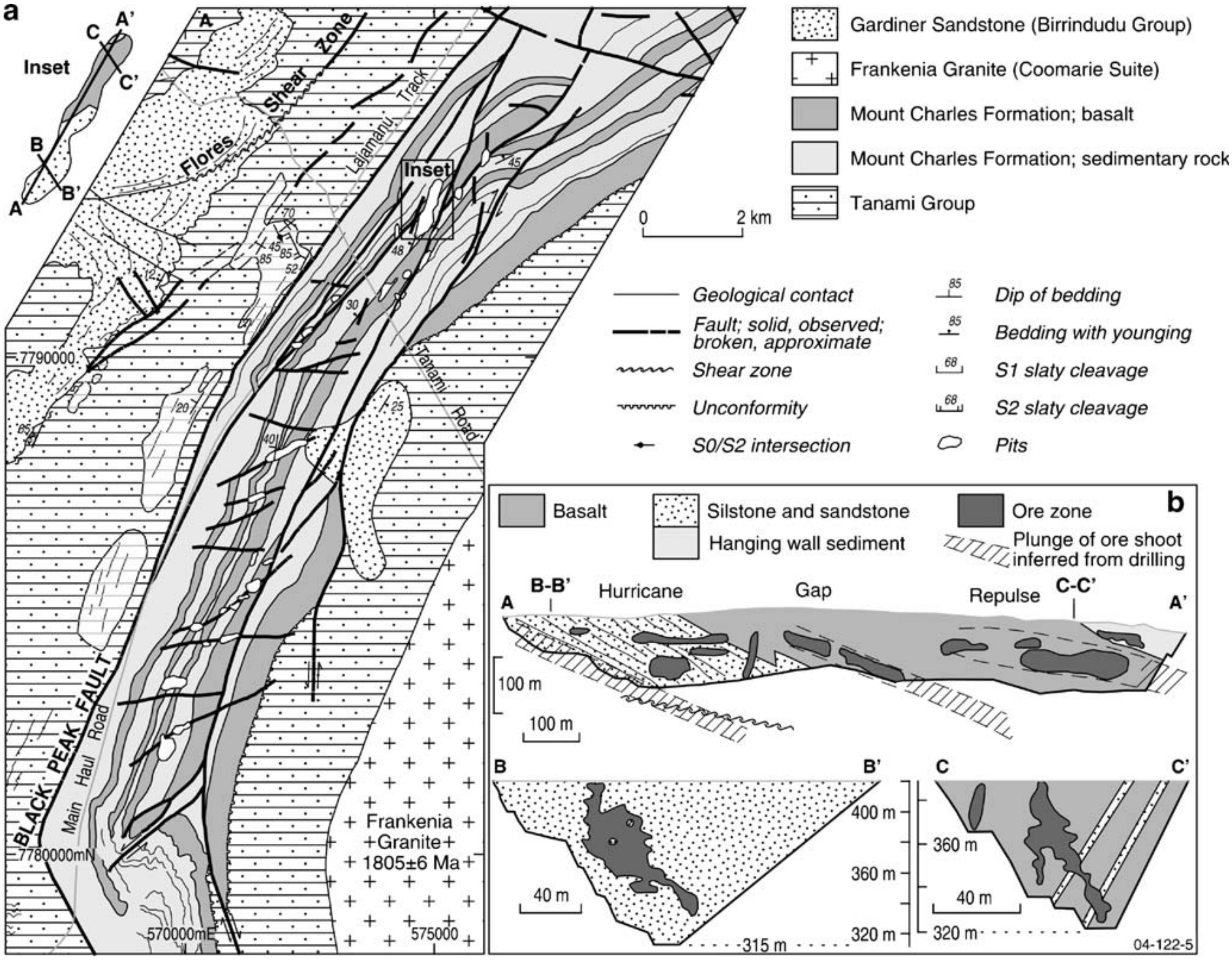

Fig. 9 Geology of the Tanami goldfield. **a** Geological plan of the goldfield, **b** sections of Hurricane-Repulse deposit (modified after Wygralak et al. 2005)

sional environment related to the Black Peak Fault. Alternatively, the Black Peak Fault may have acted as a SE-dipping oblique thrust (dextral) during regional ENE–WSW to E–W shortening (Crispe and Vandenberg 2006). The mineralized structures may have formed as subsidiary structures accommodating strain in the hanging wall to the Black Peak Fault as this fault localized deformation around a large granite-cored domain. Granite complexes have influenced the geometry of D_5 structures at the regional and local scales. Relatively small granites at The Granites goldfield may have influenced the local structural architecture and, thereby, the location and orientation of the deposits.

Although major D_5 structures were conduits of ore fluids, gold deposits did not form within these structures because high fluid fluxes overwhelmed the chemical or physical ability of these major conduits to deposit gold. Rather, ore was deposited along related second- and third-order structures where lower fluid fluxes and lower water/rock ratios allowed deposition. Such relationships are common in other lode–gold provinces (e.g., Groves et al. 1989).

As outlined above and discussed by Adams et al. (2006) and Bagas et al. (2006), structural relationships suggest an early (D_1) period of gold mineralization at The Granites and in the Bald Hill area. If this interpretation is correct, this gold event was associated with the ca. 1,830-Ma Tanami Event, the earliest orogenic event recognized in the Tanami region.

The ore fluids and their sources

Fluid inclusion studies (Mernagh and Wygralak 2006) indicate that gold mineralizing fluids ranged in temperature and salinity from 190 to 430°C and 4 to 14 eq wt% NaCl, and contained significant amounts of CO_2. With the exception of Groundrush, evidence of phase separation

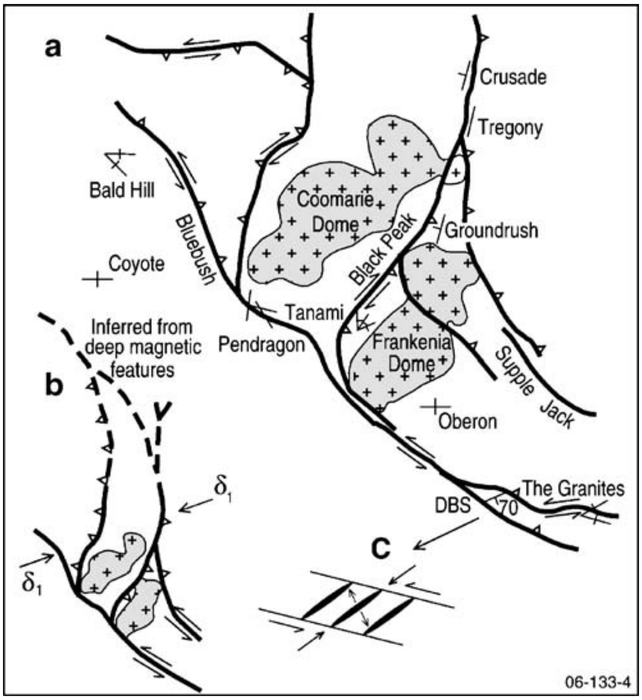

Fig. 10 Generalized diagrams for the Tanami region showing **a** the relationship of major D_5 fault/shear zones to major granite batholiths and the orientation of important veins and ore shoots (after effects of D_6 have been removed). Panel **b** shows schematic distribution of structural elements and components of proposed structural model, and **c** strain ellipse showing how east- to ENE-trending tensional veins can form in the proposed structural model. The orientations of pre-D_5 deposits (The Granites goldfield and Bald Hill areas) are shown for completeness

was noted in all deposits. Estimated depths of formation range from 1.5–5.6 km at the Tanami goldfield to 5.6–11 km at Groundrush (Table 2). Ore fluids in the Tanami goldfield contained lower quantities of CO_2 and formed veins with textures similar to those of epithermal veins (Fig. 6b,c). Although not common, these textures are widespread and closely related to gold. The origin of the Tanami goldfield fluids is debatable: alternatives include the epizonal portion of a lode–gold mineral system (Hagemann et al. 1992; Groves 1993) or a true low-sulfidation epithermal origin. The former interpretation is preferred since carbonic inclusions, which are atypical of epithermal veins (Bodnar et al. 1985), are present.

Based on oxygen and hydrogen isotopes of vein quartz and fluid inclusions, Wygralak et al. (2005) could not distinguish unambiguously the origin of the ore fluids. They demonstrated that the fluids from Callie and the Tanami goldfield overlap the fields of metamorphic and magmatic waters, but that the fluids from The Granites goldfield (based on one δD determination) overlap only the magmatic field. However, this latter interpretation is based mainly on bulk fluid inclusion δD analyses, and Adams (1997) prefers a metamorphic origin for The Granites ore

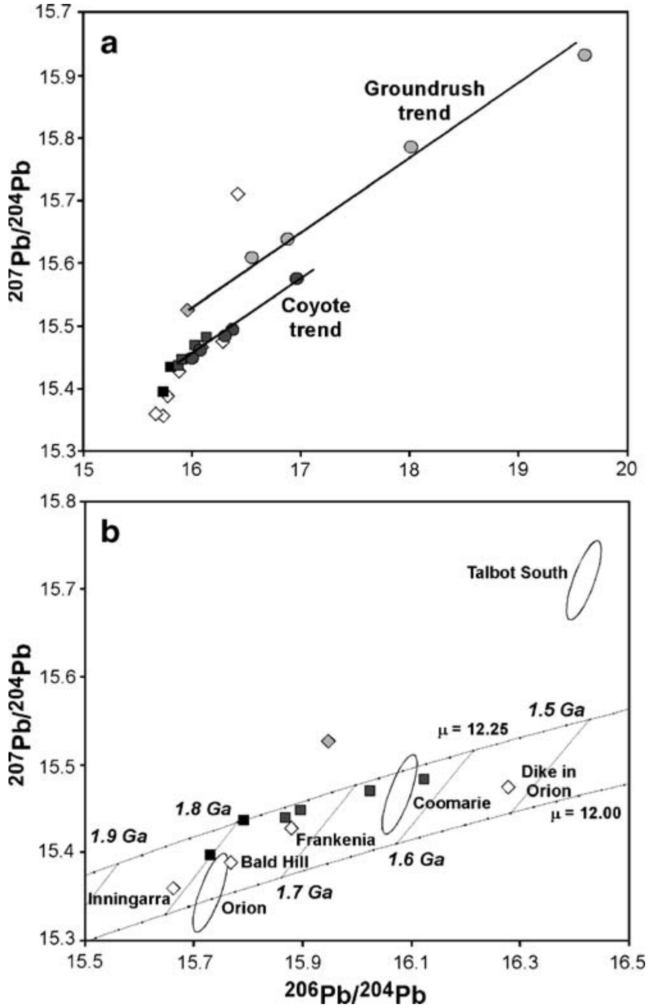

Fig. 11 $^{207}Pb/^{204}Pb$ vs $^{206}Pb/^{204}Pb$ diagrams showing the lead isotope characteristics of galena, K–feldspar, and arsenopyrite from gold deposits and granitic rocks in the Tanami region. **a** All data and **b** detailed relationship of ore lead to granite K–feldspar lead. *Diamonds* and *ellipses* indicate K–feldspar analyses, *squares* indicate galena analyses, and *circles* indicate arsenopyrite analyses. *Open symbols* indicate analyses of minerals from granites, *light gray symbols* indicate analyses from the Groundrush deposit, *dark gray symbols* indicate analyses from the Coyote and nearby deposits, and *black symbols* indicate analyses from the Callie deposit. The *lines* in **a** indicate arrays defined by disseminated arsenopyrite and ore-related K–feldspar from the Groundrush deposit and by disseminated arsenopyrite and ore-related galena from the Coyote and nearby deposits. In **b**, the *ellipses* indicate 2σ uncertainties for conventional analyses, and the *small symbols* indicate double spike and ICP-MS analyses for which the 2σ uncertainties are of similar size to the symbol. In **a**, the 2σ uncertainties are smaller than the symbols, except for single spike analyses. The modeled lead isotope evolution curves in (**b**) are modified from the model of Cumming and Richards (1975) by changing ε (to 0.07228×10^{-9} year^{-1}) to fit a K–feldspar analysis of the Inningarra Granite (1,815±4 Ma; age from Smith 2001). The K–feldspar analysis of the Inningarra granite was selected as a local control on the model as it is the least disturbed (i.e., least radiogenic) analysis of a total of seven granite K–feldspar analysis (Table 3)

fluids. Hence, available data cannot distinguish between metamorphic and magmatic origins for the ore fluid, a conundrum faced in many lode–gold provinces (Groves et al. 2003).

Although it is not possible to directly track the source of gold, the sources of lead and sulfur, which are commonly closely related to gold, can be constrained in some cases. Data in Table 3, which summarizes published sulfur isotope data (Tunks 1996; Adams 1997; Wygralak et al. 2005; Tunks and Cooke 2006; Adams et al. 2006), indicate that with one important exception ore-related sulfides from the Tanami region have a relatively restricted range in δ^{34}S, with most analyses between 4 and 10‰. The exception is the late-stage (syn- to post-D_5) sulfides at The Granites, which are characterized by lower δ^{34}S of −2 to 4‰ (Adams et al. 2006). Differences in δ^{34}S characteristics between this stage and the earlier stage (syn-D_1) support the interpretation of two mineralizing events at The Granites goldfield. Differences in δ^{34}S signatures may indicate two discrete sulfur sources.

Like hydrogen and oxygen isotopes of the ore fluids, sulfur isotopes are not diagnostic of a particular sulfur source. The δ^{34}S range of the Tanami region ore-related sulfides overlaps the extended range for magmatic sulfur identified by Ohmoto (1986). It is also consistent with the range of δ^{34}S reported in Paleoproterozoic sedimentary rocks (e.g., Canfield and Raiswell 1999). Hence, as also suggested by Adams et al. (2006), the sulfur isotope data are not diagnostic of a particular origin for the ore sulfur.

In contrast, lead isotopes constrain the source of lead in the Tanami mineral system (Table 4; Fig. 11). Wygralak et al. (2001) compared the lead isotope composition of disseminated sulfide in mafic wall rocks of the Groundrush and Carbine (Tanami goldfield) deposits with those of K–feldspar from Tanami granites. The sulfide data, along with whole rock data from altered wall rock from Groundrush, defined an array that passed above the granite K–feldspar field in ^{207}Pb/^{204}Pb vs ^{206}Pb/^{204}Pb space, leading Wygralak et al. (2001) to conclude that the lead in the disseminated sulfide (and therefore the gold in the deposits) had a different source to the lead in the granites.

However, new data from the Groundrush, Coyote, and Pebbles deposits (Table 4) suggest more complicated lead isotope relationships (Fig. 11a). Gold-related galena from the Coyote and Pebbles deposits, along with galena that paragenetically brackets gold at the Callie deposit, has broadly similar lead to that from regional granites. In detail, gold-related lead from these deposits is only slightly more evolved than lead from granite K–feldspar (Fig. 10b). Moreover, disseminated arsenopyrite from the Coyote deposit defines a trend that projects into the field-defined granite K–feldspar and gold-related galena.

At the Groundrush deposit, however, a trend defined by disseminated arsenopyrite projects above the granite K–feldspar field (as originally noted by Wygralak et al. 2001) but through the composition of gold-related K–feldspar. These data, combined with data from the Callie, Coyote, and Carbine deposits, suggest multiple provincial sources of gold-related lead in the Tanami region. Although similarities in lead isotope character of galena from the Callie and Coyote deposits could be interpreted to indicate a direct or indirect magmatic component to ore lead, data from the

Table 3 Summary of sulfur isotope data from gold deposits of the Tanami region

District/deposit/paragenetic stage	Mineral	Range in δ^{34}S (‰)	Number of analyses
Tanami (mostly Hurricane-Repulse with some from Carbine)			
Diagenetic	Pyrite	17.8–19.2	1 (C) & 7 (LA)
Stage II (pre-ore)	Pyrite	31.7–37.2	1 (C) & 7 (LA)
Stage IV (ore); in sedimentary rocks	Pyrite	6.8–10.6	6 (C) & 24 (LA)[a]
Stage IV (ore); in basalt	Pyrite	9.2–12.3	24 (LA)
Dead Bullock Soak			
Callie; disseminated in wall rock	Arsenopyrite	8.8–9.5	3 (C)
Triumph Hill; disseminated in wall rock (poor analyses)[b]	Arsenopyrite	1.0–2.0	2 (C)
Colliwobble Ridge; disseminated in wall rock	Arsenopyrite	6.4	1 (C)
Colliwobble Ridge; in ore-stage vein	Pyrite	3.9	1 (C)
Tarrant; bedded	Pyrrhotite	6.0–6.6	2 (C)
The Granites			
Syn-D_1	Arsenopyrite	6.4–8.5	33 (C)
Syn-D_1	Pyrrhotite	4.2–7.3	31 (C) & 3 (LA)[c]
Syn-D_1	Pyrite	5.9–17.4 (mostly 5.9–8.6)	4 (LA)
Syn-to post D_3	Arsenopyrite	1.8–3.6	2 (C)
Syn-to post D_3	Pyrrhotite	−2.3 to 4.0	13 (C) & 2 (LA)
Syn-to post D_3	Marcasite	2.2	1 (LA)

Data for this table were taken from Tunks (1996: Tanami goldfield), Adams (1997: The Granites goldfield), and Wygralak et al. (2005: all goldfields).

C Conventional analysis, *LA* laser ablation analysis

[a] Includes three analyses of Wygralak et al. (2005) from Carbine

[b] These analyses are of powder that contains significant silicate contamination.

[c] Includes two analyses of Wygralak et al. (2005) from Quorn

Table 4 Lead isotope analyses of sulfide minerals, K–feldspar, and whole rock from the Tanami region

Location[a]	Sample	Mineral	$\frac{^{206}Pb}{^{204}Pb}$	$\frac{^{207}Pb}{^{204}Pb}$	$\frac{^{208}Pb}{^{204}Pb}$	Lab[b]	Model age (Ma)[c]	μ[c]	Geologic age (Ma)[d]	Comments
Gold deposits										
Coyote (482385E, 7799797N)	CYDD14-199	Galena	16.024	15.470	35.732	1	1678	12.21	1793	Barren quartz vein
	16018.5	Galena	15.897	15.448	35.539	2	1738	12.22	1793	Auriferous quartz vein
	16018.10	Galena	16.124	15.483	35.773	2	1628	12.20	1793	Auriferous quartz vein
	178854	Arsenopyrite	16.954	15.578	36.685	1				Disseminated in wall rock
	178855	Arsenopyrite	15.986	15.452	35.626	1				Disseminated in wall rock
	178856	Arsenopyrite	16.289	15.487	36.005	1				Disseminated in wall rock
	178857	Arsenopyrite	16.063	15.465	35.703	1				Disseminated in wall rock
	178858	Arsenopyrite	16.360	15.497	35.869	1				Disseminated in wall rock
Pebbles (479200E, 7794200N)	16023.10	Galena	15.869	15.439	35.756	2	1749	12.21		Auriferous quartz vein
Sandpiper (485800E, 7729300N)	178833	Galena	20.913	16.095	40.186	1				In shears
Callie (597500E, 7729300N)	DBD400-573.9	Galena	15.793	15.436	35.614	1	1793	12.25	1803	Quartz vein with unclear relationship to auriferous veins
	11674	Galena	15.731	15.397	35.492	1	1801	12.16	1803	Post-gold quartz-carbonate vein
Oberon (603000E, 7756500N)	11499	K–feldspar	16.537	15.684	36.377	1	1540	12.59		Auriferous quartz vein
Carbine (Tanami goldfield: 569600E, 7781800N)	11632[e]	K–feldspar	17.443	15.721	37.447	2	1047	12.34		Auriferous quartz vein
	11598[e]	Pyrite	18.397	15.780	38.562	2				Disseminated in wall rock
	11599[e]	Pyrite	17.175	15.635	37.531	2				Disseminated in wall rock
	11662[e]	Pyrite	17.802	15.752	37.949	2				Disseminated in wall rock
Groundrush (603800E, 7820200N)	12074	K–feldspar	15.950	15.527	35.748	1	1768	12.44		Auriferous quartz vein
	11523	Arsenopyrite	16.872	15.642	37.088	3				Disseminated in wall rock
	11525	Arsenopyrite	16.539	15.612	36.688	3				Disseminated in wall rock
	11527[e]	Arsenopyrite	18.221	15.778	38.174	2				Disseminated in wall rock
	11695[e]	Whole rock	19.592	15.936	40.786	2				
	11696[e]	Whole rock	18.005	15.788	38.354	2				
	11697[e]	Whole rock	24.067	16.362	47.551	2				
Granites										
Frankenia (586766E, 7778403N)	11700	K–feldspar	15.879	15.428	35.588	3	1734	12.17	1805	
Coomarie (546122E, 7809539N)	11701	K–feldspar	16.078	15.466	35.492	2	1642	12.17	1815	
Talbot South (604048E, 7820272N)	11702	K–feldspar	16.417	15.711	36.208	2	1631	12.73	1815	
Inningara (641631E, 7725865N)	11705	K–feldspar	15.662	15.360	35.431	3	1815	12.09	1815	
Bald Hill (489106E, 7803803N)	2001082002	K–feldspar	15.767	15.389	35.466	3	1772	12.11	1795	
Orion (444761E, 7810653N)	2001082003	K–feldspar	15.730	15.356	35.353	2	1769	12.03	1793	
Dyke in Orion (444871E, 7810913N)	2001082004	K–feldspar	16.277	15.475	35.542	3	1528	12.09		

[a] UTM locations in parentheses use GDA94 datum. For deposits, the location is that stored in State Geological Survey mineral occurrence databases. For granite samples, the location is that stored in Geoscience Australia's OZROCKS database.

[b] Labs and analytical precisions (2σ expressed as) are as follows:

1 Melbourne University ICP-MS, *2* PRISE (Australian National University) double spike, *3* CSIRO conventional, *4* CSIRO double spike.

[c] Model age and μ calculated using a modified Cumming and Richards (1975) model as described in the caption to Fig. 10.

[d] Geologic ages determined from SHRIMP ages of zircons (granites: Smith 2001; Cross et al. 2004) and ore-related xenotime (gold deposits: Cross et al. 2005; J Claoue-Long, unpublished data Bagas et al. 2006).

[e] Data from Wygralak et al. (2005)

Groundrush and Carbine deposits are inconsistent with this interpretation. A more likely scenario is that the lead was leached from local sources, including granites in some cases.

The site of metal deposition

Most gold mineralization in the Tanami region is hosted by carbonaceous sedimentary rocks, iron formation, and basalt/dolerite, which have significantly different chemical and physical properties. In the following section, gold depositional mechanisms for each of these hosts are explored to identify the most important characteristics of these rocks for gold deposition.

Deposits hosted by carbonaceous, fine-grained sedimentary rocks

Carbonaceous sedimentary rocks in the Dead Bullock Formation host most of the known gold resource in the Tanami region. At the world-class Callie deposit, gold is localized where D_5 corridors of sheeted, quartz veins obliquely cut a F_1 anticlinorium. Mineralization is best developed in anticlinal fold closures where the host rocks have been bleached and decarbonized. Rocks below the ore zone are magnetite-rich. Other, smaller, deposits hosted by fine-grained clastic sedimentary rocks share many of these characteristics. The conjunction of all of these characteristics may be the main reason for the large gold accumulation at Callie. Figure 12 illustrates a genetic model for the formation of the Callie deposit based on the above characteristics.

Ground preparation

At Callie, the D_5 structural corridor, which acted as a fluid conduit, is subparallel to the F_1 axial plane and at a low angle to bedding along fold limbs. However, in anticlinal and synclinal closures, this corridor is at a high angle to bedding (Fig. 12a). Bedding along fold limbs focused fluids into anticlinal closures (Fig. 12b) where the high angle of bedding to fluid flow enhanced ore depositing chemical reactions. The fluids were focused away from synclinal closures, accounting for the lower abundance of gold in these positions. The coincidence of an E-plunging F_1 anticlinorial closure and the ENE-trending D_5 structural corridor may have been essential to form the Callie deposit. Other sediment-hosted deposits in the Tanami region, including Oberon, also are localized within preexisting anticlines, and preliminary seismic data (Goleby et al. 2006) suggest that the Groundrush deposit is associated with a thrust-related ramp anticline.

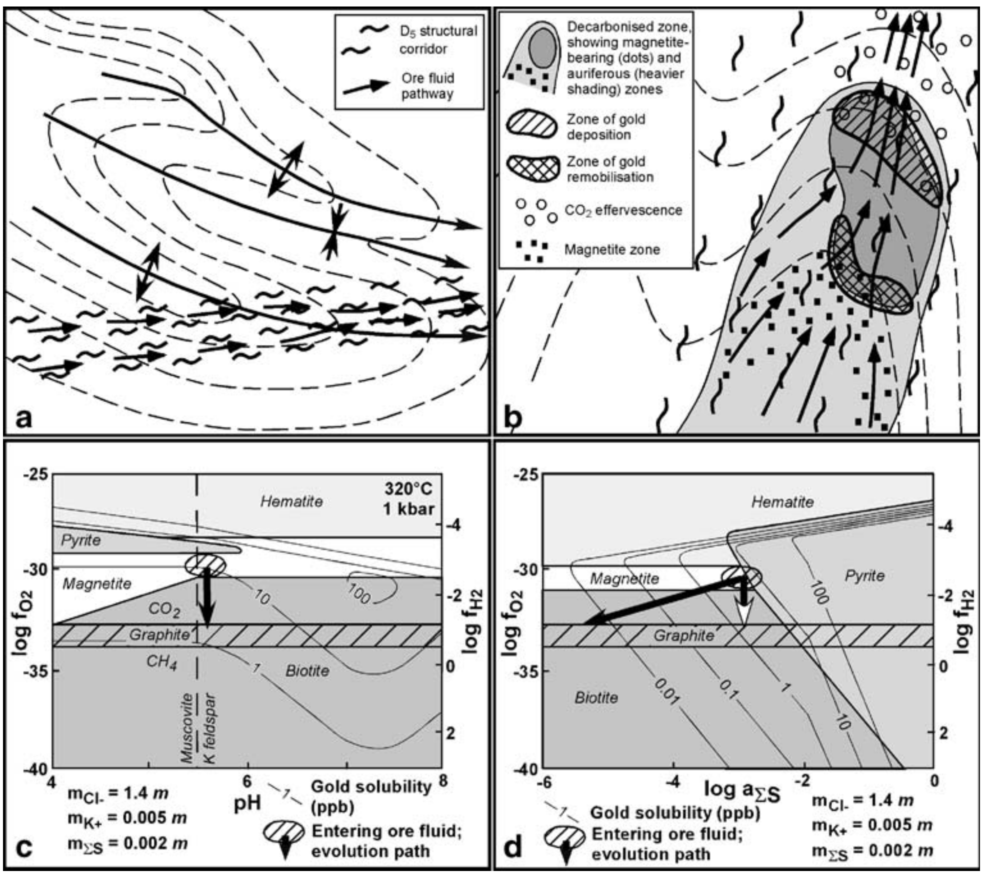

Fig. 12 Schematic diagrams illustrating the proposed genetic model for the Callie (and other carbonaceous siltstone-hosted) deposit. **a** Plan at time of mineralization, **b** cross section at time of mineralization, **c** log f_{O2}–pH diagram showing possible evolution paths of hydrothermal fluids, and **d** log f_{O2}–$a\sigma_S$ diagram showing possible evolution paths of hydrothermal fluids. The *solid arrows* in **c** and **d** illustrate the hypothesized evolution of the hydrothermal fluid during decarbonization, unmixing, and gold deposition. The *open arrow* in **d** illustrates the evolution of the fluid if only reduction is considered as the driver for gold deposition

In addition to structural preparation, carbonaceous rocks were also essential for gold deposition as the ores occur in the first carbonaceous units in the stratigraphy. Deepwater, sediment-starved conditions (Lambeck 2004) allowed the deposition of carbonaceous matter and iron-rich sediments in the Callie Member before progradation of turbiditic sandstone of the Killi Killi Formation. The chemical reactivity of these deepwater rocks predisposed them to host later gold mineralization.

Gold mineralization

The presence of magnetite (Williams 2006) below the Callie deposit suggests that the ore fluids were initially oxidized relative to graphite stability. G. Morrisson (in Smith et al. 1998), who initially recognized decarbonization as an important control on gold deposition at this deposit, inferred that reduction of the fluid associated with the oxidation of carbonaceous material as the main cause of gold deposition (e.g., Fig. 12c). Another consequence of decarbonization is the conversion of carbonaceous material to CO_2, which initially dissolved into the ore fluid:

$$C + 2H_2O \rightarrow CO_2(aq) + 2H_2(g) \quad (1)$$

In the presence of sufficient carbonaceous material, the fluid eventually saturated in CO_2 and unmixed as suggested from fluid inclusion evidence (Mernagh and Wygralak 2006). As a consequence, H_2S and H_2 in the fluid partitioned into the gas phase and gas pressure built up. H_2S loss into a gaseous phase, which decreased the concentration of aqueous H_2S in the ore fluid, possibly caused gold deposition (Fig. 12d). CO_2 unmixing (caused by decarbonization) is a more efficient mechanism for gold deposition than reduction of the ore fluids (e.g., compare paths on Fig. 12d), although both processes probably contributed to gold deposition. Loss of H_2 oxidized the ore fluid, continuously reinvigorating the reaction with carbonaceous material and CO_2 production.

The build up of gas pressure, combined with the prevailing stress conditions, eventually caused rock failure. Failure increased permeability, resulting in sheeted, dilational quartz veins. Permeability was also enhanced by volume loss caused by the removal of carbonaceous material by hydrothermal reaction, as suggested by Smith et al. (1998).

Deposits hosted by iron-rich sedimentary rocks

Iron-rich sedimentary rocks, some of which qualify as iron formation, are important hosts to lode–gold deposits, both in Archean and Proterozoic rocks. In both The Granites and Dead Bullock Soak goldfields, the host iron-rich unit is also enriched in sulfide (to 15%, including arsenopyrite, pyrrhotite, and pyrite) within ore zones. Gold occurs both in veins and in the host rock associated with disseminated sulfide minerals. Similarities of these characteristics to other Proterozoic iron-rich sediment-hosted deposits (e.g., Homestake and some Pine Creek deposits: Partington and Williams 2000) suggests similar depositional mechanisms.

Phillips and Groves (1983) and Böhlke (1988) argued that the depositional mechanism for gold in lode deposits hosted by iron-rich rocks (e.g., BIF and mafic igneous rocks) was sulfidation of the rock, which causes H_2S loss from the fluid:

$$FeO_{rock} + H_2S(aq) \rightarrow FeS + H_2O \quad (2)$$

Similar, though more complicated, reactions can be written for pyrite and arsenopyrite, all of which remove H_2S from the ore fluid. Loss of H_2S destabilizes gold thiocomplexes, leading to gold deposition. Given the abundance of replacive sulfide in the host rocks, this mechanism probably dominates gold deposition in BIF-hosted deposits.

In the Dead Bullock Soak goldfield, the main structural control on the ores is the intersection of the D_5 structural corridor with F_1 flexures and anticlinal closures. However, in The Granites goldfield, mineralization was localized by layer-parallel shears that focused on ore fluids. Although ore depositional mechanisms were probably similar in both The Granites and Dead Bullock Soak goldfields, a number of structural sites, including anticlinal closures, flexures, structurally thickened zones, or extensively sheared zones are suitable sites for ore-forming reactions.

Deposits hosted by mafic rocks

Iron-rich mafic rocks are some of the best hosts to lode–gold ores, hosting giant deposits in the Yilgarn (e.g., the Golden Mile) and other lode–gold districts around the world. Like iron-rich sedimentary rocks, wall rock sulfidation reactions have been inferred as the main mechanisms of gold deposition (e.g., Phillips and Groves 1983), and the relative competence of mafic rocks may have localized structures that focused fluid flow (Hagemann and Cassidy 2000). In the Tanami region, mafic rocks host a significant proportion of known gold, although wall rock sulfidation may not have been the cause of gold deposition.

The Groundrush deposit

The Groundrush deposit is relatively sulfide-poor, both in the veins and particularly the wall rock, where sulfide abundance rarely exceeds 1%. Despite being iron-rich and having high Fe/(Fe+Mg) (0.59–0.83, n=4), both of which favor wall rock sulfidation (Böhlke 1988), sulfidation of this rock was not the main mechanism of gold deposition.

An alternative mechanism could be the reduction of the ore fluids (e.g., Fig. 12c) that would be accompanied by oxidation of the host rocks, for which there is no evidence. Hence, it is unlikely that chemical reactions with the wall rock caused gold deposition at Groundrush.

A third alternative mechanism for gold deposition is depressurization associated with structural movement along shear zones. Sibson et al. (1988) have suggested that faults can act as valves, producing cyclical variations in fluid pressure from supralithostatic to hydrostatic. Figure 13 shows that deeper deposits such as Groundrush and Coyote are characterized by fluids with low CO_2/CH_4 ratios. These CH_4-rich fluids are more susceptible to unmixing as CH_4 is less soluble in aqueous fluids than CO_2 (Naden and Shepherd 1989). Massive rocks like dolerite (Groundrush) and poorly bedded sandstone (Coyote) may have facilitated these processes given their high competence. It may be that for more reduced CH_4-rich fluids, pressure decrease is a more effective mechanism for gold deposition, particularly at deeper levels in the crust.

The Tanami goldfield

The Tanami goldfield deposits differ from other deposits in the Tanami region in terms of the low pressure at which mineralization occurred, the CO_2-poor character of the ore fluids, and the low metamorphic grade of the host rocks. These characteristics and epithermal-like textures in the veins suggest that the Tanami goldfield deposits formed at a high crustal level.

Sericitic alteration assemblages, which can extend up to 10 m from ore shoots, are commonly strongly pyritic. This assemblage and high Fe/(Fe+Mg) of unaltered basalt (0.52–0.63, n=9) suggest that sulfidation of the host rock may have been an important depositional mechanism (Böhlke 1988). Fluid mixing trends (Mernagh and Wygralak 2006) suggest that the ore fluid mixed isothermally with an ambient, high-salinity fluid, raising a second possible depositional mechanism. The presence of high-level vein textures and fluid inclusion evidence of coexisting vapor and brine (Tunks 1996) suggest that a third mechanism of gold deposition was boiling.

The fault array, whether a Reidel array (Tunks and Cooke 2006) or subsidiary faults developed in the hanging wall to an oblique thrust faults (Crispe and Vandenberg 2006), acted as a local plumbing system, with the mechanical and chemical properties of rock units determining the hosts to gold. Discrete fault planes are best developed in more competent basalt and sandy units, whereas siltstone layers are chaotically disrupted and sheared (Crispe and Vandenberg 2004). The discrete faults in the basalt would have focused fluids into this chemically receptive unit, resulting in the bulk of the gold being hosted by basalt.

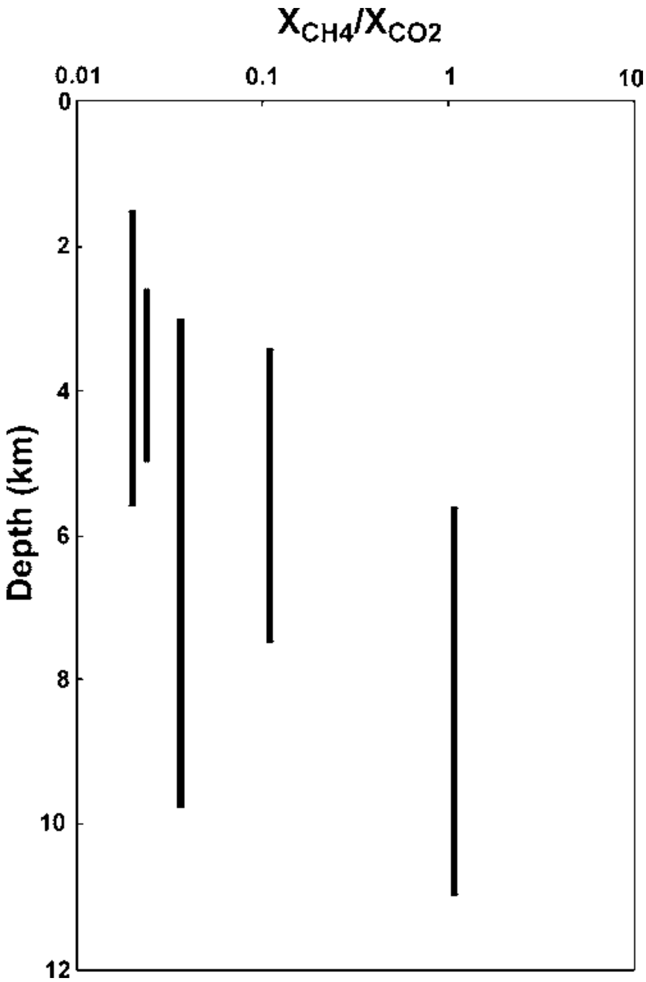

Fig. 13 Relationship between fluid CO_2/CH_4 ratios and depth for lode-gold deposits of the Tanami region (data from Mernagh and Wygralak 2006)

A genetic model for gold in the Tanami region

Figure 14 illustrates important features of the Tanami mineral system, highlighting the interplay between magmatic, metamorphic, deformation, and mineralizing processes that were critical to form Tanami lode–gold deposits. At a regional scale, essential factors include an elevated heat flow, which drove granite intrusion and fluid flow, a convergent deep-seated structural architecture that tapped the mid-crust, and the presence of granite buttresses that perturbed the stress field to localize faults.

Available data suggest that most deposits in the Tanami region formed during the latter part of a long-lived magmatic event that affected much of northern Australia. This relationship is consistent with the thermal aureole model proposed by Wall and Taylor (1990) and Wall (2005) in which gold deposits are localized within thermal aureoles of syn-ore granites. In this model, the ore fluids are sourced from dehydration reactions caused by contact metamorphism during granite intrusion. Alternatively, relationships in the Tanami region are also consistent with the model of Stüwe (1998), where emplacement of granites and gold mineralization are both products of Barrovian metamorphism in which both processes are the result of prograde metamorphic devolatilization and partial melting deeper in the crust.

Lead isotope data suggest that lead in the auriferous veins was derived from either granites or a similar source to the granites. Elevated heat flow, which produced granite melts at mid-crustal levels, would have also produced a regional metamorphic gradient. Consequently, metamorphic devolatilization at the greenschist–amphibolite transition would have produced large quantities of potential ore fluids (black, heavy arrows in Fig. 14). If these fluids were produced from rocks with the same isotopic signature as those that produced the granite melts, ores deposited from the fluids would have the same lead isotopic signature as the granites. The granites and auriferous fluid generation are symptoms of "deep-later" metamorphism (cf. Stüwe 1998).

As no definitive evidence discounts a direct granite source for the ore fluids and all isotopic data are consistent with such a source, Fig. 14 also illustrates the paths of possible magmatic–hydrothermal fluids (gray, heavy arrows). Sources for such fluids include major granite bodies exposed at the surface or much smaller bodies at depth. Like metamorphic fluids, magmatic–hydrothermal fluids would likely have been focused along D_5 faults/shears or preexisting anticlinoria (Fig. 14). Experimental and theoretical studies suggest the solubility of CO_2 in silicic melts increases with increasing pressure. As a consequence, deeper magmas evolve more CO_2-rich fluids than shallower magmas (Lowenstern 2001), suggesting deeper granites are a more likely source of CO_2-rich fluids typical of the Tanami region and other lode–gold provinces.

In any case, granites may have also played an important role in determining the geometry of the D_5 structural architecture. The north-trending faults are localized between and around the two major granite complexes, which acted as buttresses (Fig. 14). This architecture probably localized and preserved the high-level Tanami goldfield. In addition, The Granites goldfield and other smaller deposits are localized around smaller granite intrusions that may have perturbed the local stress field, forming structures that focused local fluid flow. Most importantly, the development of a network of thrust faults within an overall convergent regime tapped the mid-crust.

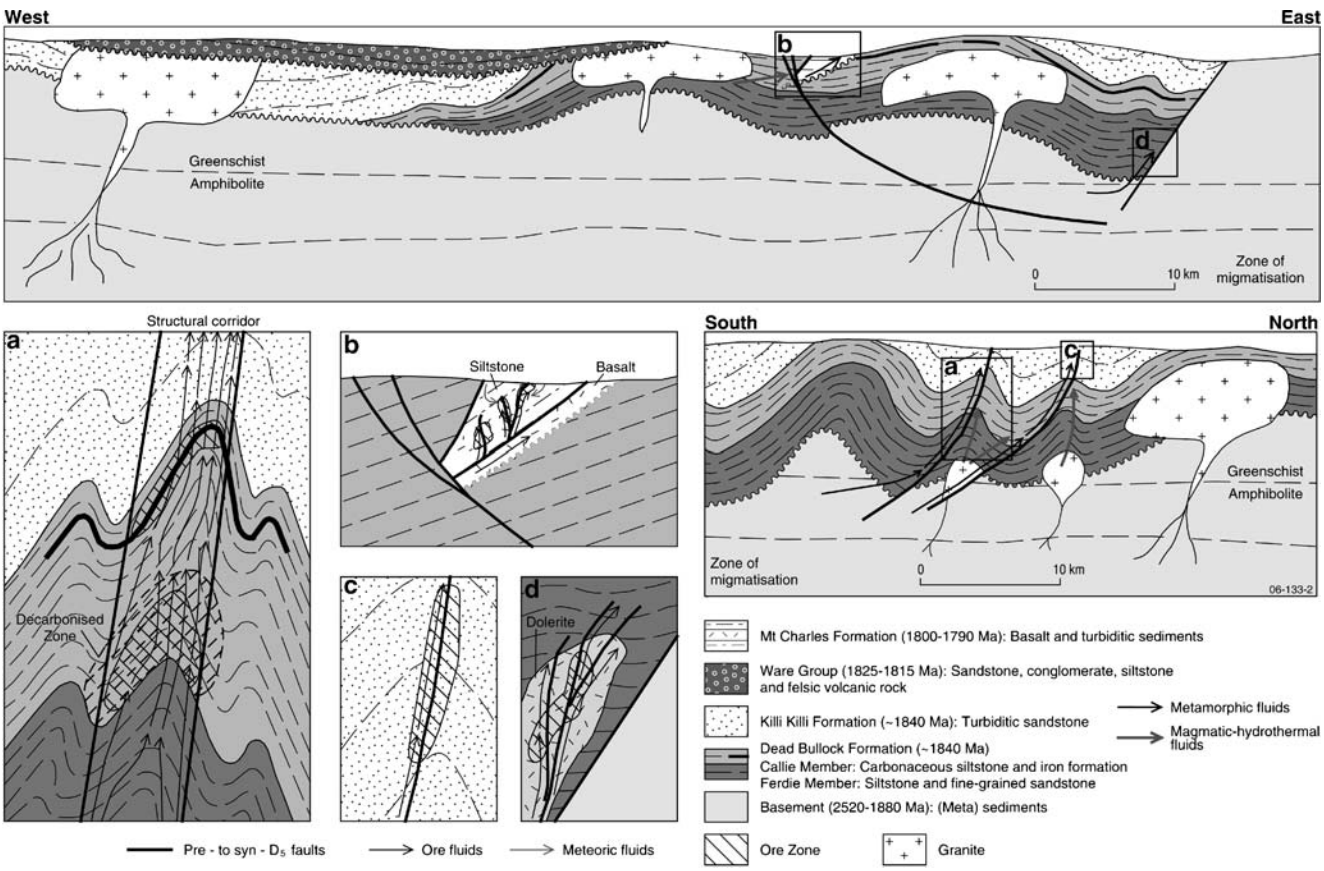

Fig. 14 Schematic diagram illustrating gold mineral systems in the Tanami region. Sections are based broadly on reflection seismic data (Goleby et al. 2006) and on inversion and forward modeling of potential field data (Meixner and Lane 2005; Vandenberg and Meixner 2003)

Local essential factors may differ spatially depending upon where in the regional architecture deposits formed. To the south and west of the Coomarie and Frankenia granite complexes, the deposits seem to form in second or third order, east-trending tensional vein arrays, particularly where these zones cut preexisting east-trending anticlinoria. Many deposits occur where these zones cut local anticlines or structurally complex/thickened zones in carbonaceous sediment rocks or iron formation (Fig. 12). As these features are most common in the Callie Member of the Dead Bullock Formation, this unit contains the largest gold resource. However, ore deposition also occurs in low-pressure zones within competent units such as sandstone of the Killi Killi Formation at the Coyote deposit.

Between and to the north of the granite complexes, the deposits appear to occur in second-order faults, dilational jogs, or zones of competency contrast that are commonly subparallel to the trend of the regional faults. Pressure drops, associated with pressure cycling in fault zones or the approach of ore fluids to the paleosurface, initiated boiling or effervescence, causing gold deposition. Chemical processes appear to be less important as depositional mechanisms in this area, although wall rock sulfidation or mixing of the ore fluids with an ambient high-salinity fluid may have assisted gold deposition in the high-level Tanami goldfield (Mernagh and Wygralak 2006).

The current understanding of the Tanami mineral system suggests that it is consistent with the continuum model originally proposed by Groves (1993). Fluid inclusion data suggest that mineralization occurred at depths from 1–2 km to as great as ~11 km (Mernagh and Wygralak 2006). In general, the deeper deposits (e.g., Groundrush) tend to be of higher temperature and more reduced (i.e., more abundant pyrrhotite and higher CH_4/CO_2) than the shallower deposits, and the shallowest deposits (e.g., Tanami goldfield) generally have low levels of carbonic gases. These variations are consistent with those that might be expected at different crustal levels in a continuum model.

Gold mineralization in the Tanami region appears to be associated with the D_1 and D_5 deformation events. D_1, which was the result of the Tanami Event, is interpreted by Crispe et al. (2006) to be an inboard response to the collision between the Kimberley and North Australian Craton. The tectonic driver to D_5 is unclear, but may be related to the shift from tectonism on the northwest margin to the southern margin of the North Australia Craton, which Crispe et al. (2006) inferred to have occurred at about 1,800 Ma.

Acknowledgements This contribution is a product from the North Australia Project, a joint National Geoscience Accord project between Geoscience Australia and the Northern Territory Geological Survey, and the Geological Survey of Western Australia. It has benefited from discussions with Richard Blewett, Paul Henson, and geologists from Newmont Australia, Tanami Gold, Barrick Australia, and Anglogold Australia and from critical reviews by Anthony Budd, David Champion, Rich Goldfarb, and David Groves. Ian Scrimgeour, Steve Sheppard, and Ian Tyler are thanked for their comments on the aspects of the evolution of the Halls Creek and Pine Creek regions relative to the Tanami region. This contribution is published with permission of the Chief Executive Officer of Geoscience Australia, the Director of the Northern Territory Geological Survey, and the director of the Geological Survey of Western Australia.

References

Adams SF (1920) A microscopic study of vein quartz. Econ Geol 15:623–664

Adams GJ (1997) Structural evolution and ore genesis of The Granites gold deposits, Northern Territory. Ph.D. Thesis, University of Adelaide

Adams GJ, Both RA, James P (2006) The Granites gold deposits, Northern Territory, Australia: evidence for an early syn-tectonic ore genesis. Miner Depos (in this issue)

Bagas L, Huston DL, Anderson J (2006) Gold deposits in the Palaeoproterozoic Tanami Group, Western Australia. Miner Depos (in this issue)

Blake DH, Tyler IM, Page RW (2000) Regional geology of the Halls Creek Orogen. Bull Aust Geol Surv Organ 246:35–62

Bodnar RJ, Reynolds TJ, Kuehn CA (1985) Fluid inclusion systematics in epithermal systems. Rev Econ Geol 2:73–97

Böhlke JK (1988) Carbonate-sulfide equilibria and “stratabound” disseminated epigenetic gold mineralization—a proposal based on examples from Allegheny, California, USA. Appl Geochem 3:499–516

Canfield DE, Raiswell R (1999) The evolution of the sulfur cycle. Am J Sci 299:97–723

Crispe A, Vandenberg L (2004) Preliminary findings from mapping in the northern Tanami. Northern Territory Geological Survey Record 2004-0001 pp 17–18

Crispe A, Vandenberg L (2006) Geology of the Tanami region, Northern Territory. Northern Territory Geological Survey Report (in press)

Crispe AJ, Vandenberg LC, Scrimgeour IR (2006) Geological framework of the Palaeoproterozoic Tanami Region, Northern Territory. Miner Depos (in this issue)

Cross AJ, Crispe AJ (2006) SHRIMP U–Pb analyses of detrital zircon: a window to understanding the early Palaeoproterozoic development of the Tanami basin, northern Australia. Miner Depos (in this issue)

Cross AJ, Claoué-Long JC, Scrimgeour IR, Close DF, Edgoose CJ (2004) Summary of results, Joint NTGS–GA geochronology project: southern Arunta Region. Northern Territory Geological Survey Record 2004-003

Cross AJ, Fletcher IF, Crispe AJ, Huston DL, Williams N (2005) New constraints on the timing of deposition and mineralisation in the Tanami Group. Annual Geoscience Exploration Seminar (AGES) 2005: record of abstracts. Northern Territory Geological Survey Record 2005-001

Cumming GL, Richards JR (1975) Ore lead isotope ratios in a continuously changing Earth. Earth Planet Sci Lett 28:155–171

Daly J (1962) Granites geophysical survey, Northern Territory, 1939. Bureau of Mineral Resources Geology and Geophysics, Australia Record 1962/154

Davidson AA (1905) Journal of exploration in central Australia by The Central Australian Exploration Syndicate. South Australian Parliamentary Paper 27

Dean AA (2001) Igneous rocks of the Tanami region. Northern Territory Geological Survey Record 2001/03
Fraser (2002) Geochronology of Tanami ores and host rocks. Annual Geoscience Exploration Seminar (AGES) 2002: record of abstracts. Northern Territory Geological Survey Record 2002/0003
Goldfarb RJ, Groves DI, Hart GJR (2001) Orogenic gold and geologic time: a global synthesis. Ore Geol Rev 18:1–75
Goleby BR, Lyons P, Huston DL, Vandenberg L, Davies B, Bagas L, Jones KEA, Smith, Gebre-Mariam M, English L, Green M, Korsch RJ, Crispe, A (2006) The 2005 Tanami seismic collaborative research project: seismic results. In: Lyons P, Huston DL (eds.) Evolution and metallogenesis of the North Australian Craton. Geoscience Australia Record 2006/16: 41–46
Green MJ (2006) Granite geochemistry, In: Geology of the Tanami region, Northern Territory. Northern Territory Geological Survey Report (in press)
Groves DI (1993) The crustal continuum model for late-Archæan lode gold deposits of the Yilgarn block, Western Australia. Miner Depos 28:366–374
Groves DI, Barley ME, Ho SE (1989) Nature, genesis, and tectonic setting of mesothermal gold mineralization in the Yilgarn Block, Western Australia. Econ Geol Monogr 6:71–85
Groves DI, Goldfarb RJ, Robert F, Hart GJR (2003) Gold deposits in metamorphic belts: overview of current understanding, outstanding problems, future research, and exploration significance. Econ Geol 98:1–29
Hagemann SG, Cassidy KF (2000) Archean orogenic lode gold deposits. Rev Econ Geol 13:9–68
Hagemann SG, Groves DI, Ridley JR, Vearncombe JR (1992) The Archean lode gold deposits at Wiluna, Western Australia: high-level brittle-style mineralization in a strike–slip regime. Econ Geol 87:1022–1053
Haines PWO, Jago JB, Gum JC (2001) Turbidite deposition in the Cambrian Kanmantoo Group, South Australia. Aust J Earth Sci 48:465–478
Hassan LY (2002) Mineral occurrences and exploration potential of the east Kimberley. Geological Survey of Western Australia Report 74
Hodgson CJ (1993) Mesothermal lode gold deposits. Geol Assoc Can (Special Paper) 40:635–678
Hodgson CJ, MacGeehan PJ (1982) Geological characteristics of gold deposits in the Superior Province of the Canadian Shield. CIM Spec Vol 24:211–229
Hossfeld PS (1940a) Preliminary report on The Granites goldfield, central Australia. Aerial Geology and Geophysics Survey of Northern Australia, Northern Territory Report 30
Hossfeld PS (1940b) The gold deposits of The Granites–Tanami district, central Australia. Aerial Geology and Geophysics Survey of Northern Australia, Northern Territory Report 43
Ireland TJ, Mayer TE (1984) The geology and mineralisation of The Granites gold deposits, Northern Territory. Proceedings of the Australasian Institute of Mining and Metallurgy Conference, Darwin, Northern Territory, pp 397–405
Jagodzinki EA (1998) Shrimp U–Pb dating of ignimbrites in the Pul Pul Rhyolite, Northern Territory; a cautionary tale. AGSO Res Newsl 28:23–25
Lambeck L (2004) Sequence stratigraphic framework of mineralised units in the Tanami region. Annual Geoscience Exploration Seminar (AGES) 2004: record of abstracts. Northern Territory Geological Survey Record 2004-001
Lowenstern JB (2001) Carbon dioxide in magmas and implications for hydrothermal systems. Miner Depos 36:490–502
Mayer TE (1990) The Granites gold field. Aus IMM Monogr 14:715–719
Meixner AJ, Lane R (2005) 3D inversion of gravity and magnetic data for the Tanami Region. Annual Geoscience Exploration Seminar (AGES) 2005: record of abstracts. Northern Territory Geological Survey Record 2005-001
Mernagh TP, Wygralak AS (2006) Ore fluids of the Tanami region. Miner Depos (in this issue)
Morelli RM, Creaser RA, Bell CC (2005) Re–Os geochronology of the Homestake gold deposit, Black Hills, South Dakota, and implications for chronometer closure temperature. Geological Society of America Abstracts with Programs 37:452
Naden J, Shepherd T (1989) Role of methane and carbon dioxide in gold deposition. Nature 342:793–795
Nicholson PM (1990) Tanami gold deposit. Aus IMM Monogr 14:719–724
Ohmoto H (1986) Stable isotope geochemistry of ore deposits. Rev Miner 16:491–559
Ord River Minerals (2005) Activities report, quarter ended 30 September 2005. Announcement to Sydney Stock Exchange, 31 October 2005
Page R, Sun S-S, Blake D (1995) Geochronology of an exposed late Archæan basement terrane in The Granites–Tanami region. AGSO Res Newsl 22:19–20
Partington GA, Williams PJ (2000) Proterozoic lode gold and (iron)–copper–gold deposits: a comparison of Australian and global examples. Rev Econ Geol 13:69–101
Phillips GN, Groves DI (1983) The nature of Archæan gold-bearing fluids as deduced from gold deposits of Western Australia. J Geol Soc Aust 30:25–39
Plumb KA (1990) Halls Creek Province and The Granites–Tanami Inlier-regional geology and mineralisation. Aust IMM Monogr 14:681–695
Rasmussen B, Sheppard S, Fletcher IR (2006) Testing ore deposit models using in situ U–Pb geochronology of hydrothermal monazite: Paleoproterozoic gold mineralization in northern Australia. Geology 34:77–80
Scrimgeour I, Sandiford M (1993) Early Proterozoic metamorphism at The Granites gold mine, Northern Territory: implications for the timing of fluid production in high-temperature, low-pressure terranes. Econ Geol 88:1099–1113
Şener AK, Young C, Groves DI, Krapež B, Fletcher IR (2005) Major orogenic gold episode associated with Cordilleran-style tectonics related to the assembly of Paleoproterozoic Australia? Geology 33:225–228
Sheppard S, Tyler IM, Griffin TJ, Taylor WR (1999) Palaeoproterozoic subduction-related and passive margin basalt in the Halls Creek Orogen, northwest Australia. Aust J Earth Sci 46:679–690
Sheppard S, Griffin TJ, Tyler IM, Page R (2001) High- and low-K granites and adakites at a Palaeoproterozoic plate boundary in northwestern Australia. J Geol Soc (Lond) 158–547–560
Sibson RH, Robert F, Poulsen KH (1988) High-angle reverse faults, fluid–pressure cycling, and mesothermal gold–quartz deposits. Geology 16:551–555
Smith JB (2001) Summary of results. Joint NTGS–AGSO age determination program 1999–2001. Northern Territory Geological Survey Record 2001-007
Smith EH, Lovett DR, Pring PI, Sando BG (1998) Dead Bullock Soak gold deposits. Aust IMM Monogr 22:449–460
Stuart-Smith PG, Needham RS, Page RW, Wyborn LAI (1993) Geology and mineral deposits of the Cullen Mineral Field, Northern Territory. Bull Aust Geol Surv Organ 229
Stüwe K (1998) Tectonic constraints on the timing relationships of metamorphism, fluid production, and gold-bearing emplacement. Ore Geol Rev 13:219–228
Tunks AJ (1996) Geology of the Tanami Gold Mine, Northern Territory. Ph.D. Thesis, University of Tasmania
Tunks AJ, Cooke DR (2006) Geology and structural controls on mineralization at the Tanami gold mine. Miner Depos (in this issue)
Tunks AJ, Marsh S (1998) Gold deposits of the Tanami Corridor. Aust IMM Monogr 22:443–448

Vallini DA, Groves DI, McNaughton NJ, Fletcher IR (2006) Uraniferous authigenic xenotime in northern Australia and its relationship to unconformity-associated uranium mineralization. Miner Depos (in this issue)

Vandenberg LC, Meixner AJ (2003) The Tanami 3D model. Annual Geoscience Exploration Seminar (AGES) 2003: record of abstracts. Northern Territory Geological Survey, Record GS 2003-0001

Vandenberg LC, Hendrickx MH, Crispe AJ (2001) Structural geology of the Tanami region. Northern Territory Geological Survey Record 2001-004

Voulgaris P, Emslie J (2004) Geology and ore estimation at the Callie underground gold mine, Tanami, NT. The Aus IMM Bull 2:71–78

Wall VJ (2005) TAG:Thermal aureole (pluton-related) gold systems. AIG News 79:1–7

Wall VJ, Taylor JR (1990) Granite emplacement and temporally related gold mineralisation. Geological Society of Australia Abstracts 25:264–265

Williams NC (2006) Controls on mineralization at the world-class Callie gold deposit, Tanami desert, Northern Territory, Australia. Miner Depos (in this issue)

Wygralak AS, Mernagh TP, Fraser GF, Huston DL, Denton G, McInnes B, Crispe A, Vandenberg L (2001) Gold mineral systems in the Tanami region. AGSO Res Newsl 34:2–14

Wygralak AS, Mernagh TP, Huston DL, Ahmad M (2005) Gold mineral system of the Tanami region. Northern Territory Geological Survey Report 2004/18